# SOUNDREACTOR: FRAME-LEVEL ONLINE VIDEO-TO-AUDIO GENERATION

**Anonymous authors**Paper under double-blind review

000

001

003 004

006

008 009

010 011

012

013

014

016

017

018

019

021

024

025

026

027

028

029

031

032

034

037

038

040

041

043

044

046

047

048

051

052

### **ABSTRACT**

Prevailing Video-to-Audio (V2A) generation models operate offline, assuming an entire video sequence or chunks of frames are available beforehand. This critically limits their use in interactive applications such as live content creation and emerging generative world models. To address this gap, we introduce the novel task of frame-level online V2A generation, where a model autoregressively generates audio from video without access to future video frames. Furthermore, we propose SoundReactor, which, to the best of our knowledge, is the first simple yet effective framework explicitly tailored for this task. Our design enforces end-to-end causality and targets low per-frame latency with audio-visual synchronization. Our model's backbone is a decoder-only causal transformer over continuous audio latents. For vision conditioning, it leverages grid (patch) features extracted from the smallest variant of the DINOv2 vision encoder, which are aggregated into a single token per frame to maintain end-to-end causality and efficiency. The model is trained through a diffusion pre-training followed by consistency fine-tuning to accelerate the diffusion head decoding. On a benchmark of diverse gameplay videos from AAA titles, our model successfully generates semantically and temporally aligned, high-quality full-band stereo audio, validated by both objective and human evaluations, at low per-frame token-level latency (26.6ms for the head NFE=1, 30.3ms for NFE=4 with 30FPS, 480p videos using a single H100.). Demo samples are available at https://anonymous-sr-submission.github.io/.

# 1 Introduction

Video-to-Audio (V2A) generation, the task of generating semantically and temporally aligned, high-quality audio from videos, is an extensive research area driven not only by its fundamental multimodal alignment challenges but also by its wide range of real-world applications, such as film production, video content creation, and game development (Luo et al., 2023; Du et al., 2023; Mei et al., 2024b; Zhang et al., 2024; Wang et al., 2024b;a; Viertola et al., 2025; Cheng et al., 2025; Zhong et al., 2025; Liu et al., 2025). Recent advances have led to models capable of generating high-fidelity audio with strong audio-visual synchronization (Cheng et al., 2025; Liu et al., 2025). However, the prevailing paradigm operates in an offline setting, assuming that an entire video sequence or chunks of frames are available in advance. This fundamentally limits their use in frame-level online applications.

In addition to limiting online applications in live content creation, this offline constraint also becomes critical in the context of world models, which generate video sequences in an online manner from frame-level conditions (Schmidhuber, 1990; Ha & Schmidhuber, 2018; Bruce et al., 2024; Baldassarre et al., 2025; Ball et al., 2025). Recent models, such as Genie 3 (Ball et al., 2025), can generate video frames in real-time (Ball et al., 2025; Microsoft, 2025; He et al., 2025; Li et al., 2025a), yet they remain silent, operating solely in the pixel domain. Since audio and vision are tightly coupled in both real and simulated worlds, extending world models to the audio-visual domain could broaden their applicability to entertainment, education, and interactive world simulation for robotics (Chen et al., 2020a; Liu et al., 2024b; NVIDIA et al., 2025), open-ended learning (Team, 2021), and agent training (Chen et al., 2022a; Team, 2024). To bring sound to these worlds requires moving beyond the offline assumption toward a new paradigm of frame-level conditioned online general audio generation.

To address this, we introduce the novel task of frame-level online V2A generation, where a model autoregressively generates audio corresponding to a video stream without accessing future

055

056 057

060

065

066 067

068

069

070

071

072

073

074

075

076

077

079

081

083

084

085

086

087

880

089

090

091

092

093

094

095

096

098

099

100

101 102

103

104 105 106

107

Figure 1: Our scope is frame-level online video-to-audio (V2A) generation task, where future video frames are not available in advance. This contrasts with conventional offline V2A task, where an entire video sequence or chunk of frames is available in advance.

frames (See Figure 1). The online setting imposes additional unique challenges beyond those inherent to the offline setting 1: 1). End-to-end causality: The entire autoregressive (AR) framework, including the vision encoding, should be causal, as future video frames are inaccessible beforehand, 2). Low per-frame latency: models should generate audio at low per-frame latency for real-time interactive applications. Notably, even state-of-the-art V2A systems that use AR models (e.g., V-AURA (Viertola et al., 2025)) do not enforce end-to-end causality on their vision encoders (We refer to Section 4.2 and Appendix A for more details.).

To tackle these challenges, we introduce SoundReactor, the first simple yet effective framework tailored for the frame-level online V2A task on full-band stereo audio. Our design is driven by three essential properties: end-to-end causality, low per-frame latency, and high-quality audio generation with semantic and temporal audio-visual alignment. Our framework consists of an image encoder, a waveform encoder, and a causal, decoder-only multimodal Transformer (Vaswani et al., 2017) with a diffusion head (Li et al., 2024) (See Figure 2). For the image encoder, we introduce a novel conditioning scheme based on a pretrained DINOv2 encoder (Oquab et al., 2024) (Figure 2 (a)). We extract spatial grid (patch) features from each frame, a process that is inherently causal. The availability of its lightweight variants (e.g., 21M parameters) contributes to low per-frame latency for vision encoding. Moreover, we further augment these grid features with temporal differences, providing both semantic and temporal information to the generative model backbone. For continuous audio latents, we utilize a Variational Autoencoder (VAE) (Kingma & Welling, 2014) (Figure 2 (b)). We choose continuous latents for two reasons. First, for complex data such as full-band stereo audio, continuous representations tend to yield superior reconstruction quality over discrete counterparts at the same temporal downsampling rate (Lan et al., 2024), which is crucial for the final generation quality <sup>2</sup>. Second, by representing each frame with a single audio latent, it simplifies AR modeling compared to predicting multiple code indices per frame as typically required by residual vector quantization (RVQ)-based tokenizers (Kumar et al., 2023; Défossez et al., 2023; Li et al., 2025b). Finally, to reduce inference latency, we accelerate the diffusion head with Easy Consistency Tuning (ECT) (Geng et al., 2025b).

We demonstrate the efficacy of SoundReactor on the OGameData dataset (Che et al., 2025), a large-scale dataset of diverse AAA gameplay videos, motivated by the field of world models. Through our experiments, we show that our model generates semantically and temporally synchronized, high-quality, full-band stereo audio under the end-to-end causal constraint. This performance is validated by both objective and human evaluations and achieved with low per-frame token-level latency (26.6ms with the head NFE=1 and 30.3ms with NFE=4), measured on 480p, 30FPS videos using a single H100 GPU.

### Our main contributions are:

• We introduce the frame-level online V2A generation task, a new paradigm as a key step toward interactive multimodal applications.

<sup>&</sup>lt;sup>1</sup>e.g., generating high-quality audio with strong semantic and temporal audio-visual alignment.

<sup>&</sup>lt;sup>2</sup>While the reconstruction quality of discrete tokenizers can be improved by increasing their bitrate, training high-bitrate tokenizers is a non-trivial task.

- We propose SoundReactor, which is, to our knowledge, the first framework explicitly tailored
  to this task, featuring a novel visual conditioning scheme and continuous audio latents for
  AR generation with an accelerated diffusion head.
- We demonstrate that SoundReactor achieves notable V2A generation performance under the end-to-end causal constraint while maintaining low per-frame token-level latency.

# 2 PRELIMINARIES

### 2.1 DIFFUSION MODELS

Let  $p_{\rm data}$  denote the data distribution. In Diffusion Models (DMs) (Ho et al., 2020), a clean sample  $\mathbf{x}^0 \sim p_{\rm data}$  is generated through an iterative denoising process, beginning from a Gaussian prior  $p_T$ . When the forward diffusion process is defined by  $\mathrm{d}\mathbf{x}^t = \sqrt{2t}\,\mathrm{d}\mathbf{w}_t$ , initialized by  $\mathbf{x}^0$ , where  $\mathbf{w}_t$  is the standard Wiener process in forward-time (Karras et al., 2022; 2024), the deterministic counterpart of the denoising process, called the Probability Flow Ordinary Differential Equation (PF-ODE) (Song et al., 2021), is formulated as

$$\frac{\mathrm{d}\mathbf{x}^t}{\mathrm{d}t} = -t\nabla \log p_t(\mathbf{x}^t). \tag{1}$$

Typically, DMs are trained by minimizing a Denoising Score Matching (DSM) objective (Vincent, 2011; Song et al., 2021) expressed as:

$$\mathbb{E}_{\mathbf{x}^0,t,\epsilon}[\|\mathbf{x}^0 - D_{\boldsymbol{\theta}}(\mathbf{x}^t,t)\|_2^2],\tag{2}$$

where  $\epsilon \sim \mathcal{N}(\mathbf{0}, \mathbf{I})$ ,  $\mathbf{x}^t = \mathbf{x}^0 + t \, \epsilon$ , and  $D_{\theta}(\mathbf{x}^t, t)$  is a neural approximation of a denoiser function  $\mathbb{E}_{p_{0|t}(\mathbf{x}^0|\mathbf{x}^t)}[\mathbf{x}^0|\mathbf{x}^t] = \mathbf{x}^t + t^2 \nabla \log p_t(\mathbf{x}^t)$  (Efron, 2011).

### 2.2 AUTOREGRESSIVE MODELING WITHOUT DISCRETE TOKENIZATION

AR V2A generation models have been typically implemented on discrete tokens (Iashin & Rahtu, 2021; Sheffer & Adi, 2023; Mei et al., 2024b; Du et al., 2023; Viertola et al., 2025) (A broader literature review of V2A generation models is provided in Appendix A.1.) In contrast, several recent works decouple discrete tokenization from AR modeling (Li et al., 2024; Tschannen et al., 2025b;a). Specifically, MAR (Li et al., 2024) models per-token conditional distributions via a DM. Our framework builds on MAR, and we decode one token (here, a continuous-valued latent<sup>3</sup>) at a time in chronological order. We refer to this sampling variant as MAR throughout<sup>4</sup>.

Below, we outline both sampling and training procedures of MAR. Let  $\mathbf{z}_i \in \mathbb{R}^{c_z}$  denote an output vector by an AR model  $F_{\phi}$  at position i. Decoding in MAR proceeds in two stages. First, the conditioning vector  $\mathbf{z}_i$  is estimated by previous tokens:  $\mathbf{z}_i = F_{\phi}(<\text{BOS}>, \mathbf{z}_1, \dots, \mathbf{z}_{i-1})$ , where <BOS> is a start token to generate  $\mathbf{z}_1$ . Second, a vector  $\mathbf{x}_i^0$  is sampled from the probability  $q(\mathbf{x}_i^0 \mid \mathbf{z}_i)$  via an iterative denoising procedure (e.g., Eq. 1) using a trained conditional denoiser  $D_{\theta}(\mathbf{x}_i^t, t, \mathbf{z}_i)$ .

For training, the AR model  $F_{\phi}$  and the diffusion head  $D_{\theta}$  are jointly trained by minimizing a diffusion loss (Ho et al., 2020). In this work, we employ the following DSM objective based on EDM (Karras et al., 2022; 2024):

$$\mathcal{L}(\boldsymbol{\theta}, \boldsymbol{\phi}) = \mathbb{E}_{\mathbf{x}^0, t, \boldsymbol{\epsilon}} \left[ \sum_{i=1}^n \left\| \mathbf{x}_i^0 - D_{\boldsymbol{\theta}}(\mathbf{x}_i^t, t, \mathbf{z}_i) \right\|_2^2 \right].$$
 (3)

### 2.3 Easy Consistency Tuning

Despite their success, DMs are slow at sampling, often requiring tens to hundreds of steps to generate a single sample. This limitation is particularly severe for our frame-level online V2A setting, where the AR model with the diffusion head incurs non-negligible per-frame latency. To address the slow generation of DMs, substantial community efforts have been made to reduce the number of sampling steps while preserving quality (Song et al., 2023; Song & Dhariwal, 2024; Lu & Song, 2025; Geng

<sup>&</sup>lt;sup>3</sup>Unless otherwise stated, we denote "token" as a continuous-valued latent.

<sup>&</sup>lt;sup>4</sup>The original MAR predicts tokens autoregressively with various protocols.

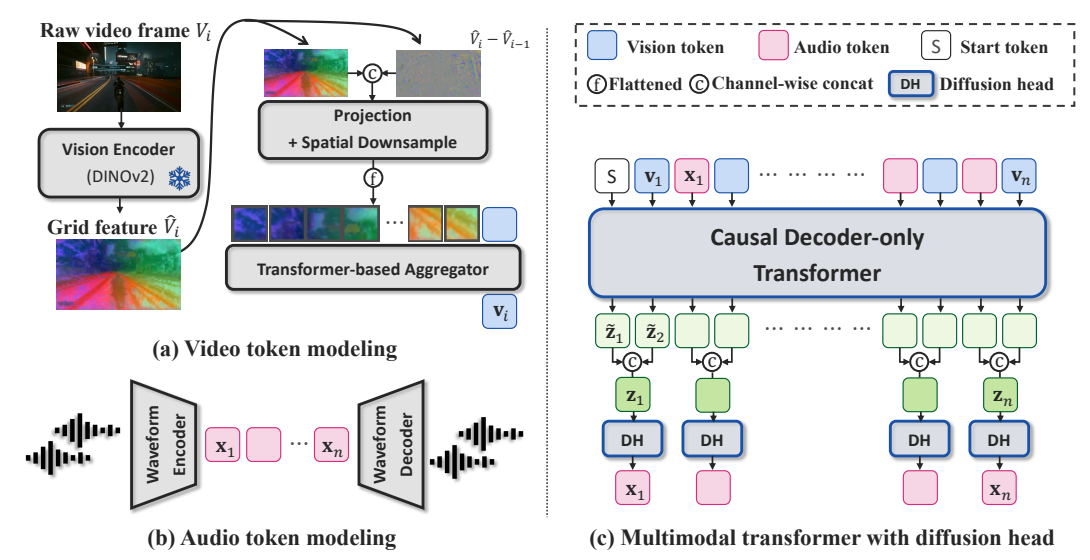


Figure 2: Overview of SoundReactor. Our framework has three components: (a) Video token modeling, (b) Audio token modeling, and (c) Multimodal AR transformer with diffusion head.

et al., 2025b; Kim et al., 2024; Zhou et al., 2025; Geng et al., 2025a; Saito et al., 2025; Novack et al., 2025b;a; Bai et al., 2024).

Within the family of Consistency Models (CMs) (Song et al., 2023; Song & Dhariwal, 2024; Lu & Song, 2025), ECT (Geng et al., 2025b) smoothly interpolates from DMs to CMs by progressively tightening the consistency condition, thereby bootstrapping a pretrained DM into a CM. It further shows that initializing a CM with a pretrained DM yields superior performance under a smaller training budget.

CMs are grounded in the PF-ODE (Eq. 1) and learn a consistency function  $G_{\theta}(\mathbf{x}^t, t)$  that maps a noisy sample  $\mathbf{x}^t$  back to its clean data  $\mathbf{x}^0$  as  $G_{\theta}(\mathbf{x}^t, t) = \mathbf{x}^0$ . In ECT,  $G_{\theta}(\mathbf{x}^t, t)$  is trained by minimizing the following objective:

$$\mathbb{E}_{\mathbf{x}^0,t,r,\epsilon} \left[ w(t) d \left( G_{\theta}(\mathbf{x}^t,t), G_{\text{sg}(\theta)}(\mathbf{x}^r,r) \right) \right], \tag{4}$$

where t > r > 0,  $\mathbf{x}^t = \mathbf{x}^0 + t\,\boldsymbol{\epsilon}$ ,  $\mathbf{x}^r = \mathbf{x}^0 + r\,\boldsymbol{\epsilon}$ , w(t) is a weighting function,  $\mathrm{sg}(\boldsymbol{\theta})$  indicates an exponential moving average (EMA) of the past values of  $\boldsymbol{\theta}$ , and d is a metric function. During training,  $\Delta t = t - r$  start large (DMs) and is gradually annealed toward 0 (CMs). Note that  $\mathbf{x}^t$  and  $\mathbf{x}^r$  are using shared noise  $\boldsymbol{\epsilon}$ .

# 3 SOUNDREACTOR

### 3.1 PROBLEM SETUP: FRAME-LEVEL ONLINE VIDEO-TO-AUDIO GENERATION

Motivated by Section 1, we aim to train a frame-level online V2A generator. Given sequences of audio tokens  $\{\mathbf{x}_1,\ldots,\mathbf{x}_n\}$  and video tokens  $\{\mathbf{v}_1,\ldots,\mathbf{v}_n\}$ , where  $\mathbf{x}_i\in\mathbb{R}^{c_\mathbf{x}}$  and  $\mathbf{v}_i\in\mathbb{R}^{c_\mathbf{v}}$  denote frame-indexed vectors for  $i=1,\ldots,n$ , the frame-level online V2A task is to model the conditional distribution of audio given video frames under an end-to-end causal constraint:

$$p(\mathbf{x}_{1:n} \mid \mathbf{v}_{1:n}) := \prod_{i=1}^{n} p(\mathbf{x}_i \mid \mathbf{x}_{< i}, \, \mathbf{v}_{\le i}).$$
 (5)

We aim to train a simple yet effective generator that models  $p(\mathbf{x}_i \mid \mathbf{x}_{< i}, \mathbf{v}_{\le i})$ , where the video tokens are provided in an online manner, i.e., an entire pipeline cannot access future video frames in advance, as illustrated in Figure 1. Throughout the paper, our models are based on continuous-valued tokens for both audio and video. In this work, we assume a frame-aligned pairing between tokens (i.e.,  $\mathbf{x}_i$  and  $\mathbf{v}_i$  refer to the same time frame.).

### 3.2 Modeling Framework

We first outline an overview of SoundReactor, then describe each component and the motivation behind its design.

**Model overview** Figure 2 summarizes SoundReactor. Our framework has three components: (a) Video token modeling: a pretrained vision encoder projects each video frame  $V_i \in \mathbb{R}^{H \times W \times 3}$  to a single aggregated token  $\mathbf{v}_i$ ; (b) Audio token modeling: a VAE encodes full-band stereo waveforms into a sequence of continuous-valued tokens  $\mathbf{x}_i$ ; and (c) Multimodal AR transformer with diffusion head: frame-aligned, interleaved audio-visual tokens are fed into a causal decoder-only transformer trained with a next-token prediction by an EDM2-style DSM loss.

Video token modeling Figure 2 (a) depicts our video token modeling. We adopt a pretrained DINOv2 vision encoder (Oquab et al., 2024) to extract grid (patch) features  $\hat{V}_i \in \mathbb{R}^{H' \times W' \times c_{\text{dinov2}}}$  per video frame. To inject temporal cues, each frame's features are then concatenated with their temporal difference from the previous frame ( $\hat{V}_i - \hat{V}_{i-1}$ ) along the channel dimension. These features pass through a projection layer with a 2D convolutional downsampler and are then flattened. We then prepend a learnable aggregation token and feed this sequence to a shallow transformer aggregator, yielding a single token  $\mathbf{v}_i$  per frame. We use grid features instead of the encoder's [CLS]-token because, in our preliminary analysis, [CLS]-token lacked temporal cues needed for audio-visual synchronization (described in more detail in Appendix B.1). We choose DINOv2 for its availability of a lightweight variant (21 M parameters) for encoding efficiency and for its rich semantic representations (Ranzinger et al., 2024). Note that leveraging pretrained DINOv2 and its grid features from vision encoders as video conditioning for V2A generation remains underexplored.

**Audio token modeling** Figure 2 (b) provides our audio token modeling. Following the VAEs from Stable Audio (SA) series (Evans et al., 2025; 2024), we compress stereo 48 kHz waveforms into a sequence of audio tokens  $\mathbf{x}_i$ . Since the original SA-VAE is not trained at 48 kHz, we train it from scratch. Using continuous-valued tokens brings two benefits for AR audio generation. First, without discrete tokenization (Kumar et al., 2023; Défossez et al., 2023; Li et al., 2025b), reconstruction quality is typically higher at the same temporal downsampling rate (Lan et al., 2024). Second, AR modelings can be simplified because waveform VAEs represent each time frame with a single latent, allowing AR models to sample one token per frame. In contrast, especially in the full-band general audio settings, discrete tokenizers commonly rely on RVQ, which typically requires AR models to predict multiple code indices per frame (Copet et al., 2023; Défossez et al., 2024).

Multimodal transformer with diffusion head In Figure 2 (c), we present the framework of the multimodal causal decoder-only transformer with the diffusion head. We feed frame-aligned, interleaved audio-visual continuous-valued tokens into the model. The AR backbone follows LLaMA-style design (Touvron et al., 2023a;b), applying pre-normalization using RMSNorm (Zhang & Sennrich, 2019), SwiGLU activation (Shazeer, 2020), and rotary positional embeddings (RoPE) (Su et al., 2024). The diffusion head largely follows the original architecture in MAR. We follow the EDM2 (Karras et al., 2024) training framework for a DSM loss; accordingly, we add a simple one-layer MLP to parameterize an uncertainty function, which we describe in Section 3.3. To obtain conditional token  $\mathbf{z}_i$ , which is fed to the diffusion head, we first conduct channel-wise concatenation  $\mathbf{z}_i = \mathtt{Concat}(\tilde{\mathbf{z}}_{2i-1}, \tilde{\mathbf{z}}_{2i})$ , where  $\tilde{\mathbf{z}}_{2i-1}$  and  $\tilde{\mathbf{z}}_{2i}$  are the outputs of transformer depicted in Figure 2 (c). By following MAR, we then project  $\mathbf{z}_i$  to the head's channel dimension.

### 3.3 TRAINING FRAMEWORK

**Stage 1: Diffusion pretraining** We first pretrain the model with a next-token prediction by minimizing a DSM objective under the EDM2 framework. The overall training loss is formulated as:

$$\mathcal{L}_{\text{Stage I}}(\boldsymbol{\theta}, \boldsymbol{\phi}) = \mathbb{E}_{\mathbf{x}^{0}, t, \boldsymbol{\epsilon}} \left[ \lambda(t) e^{-u_{\boldsymbol{\theta}}(t)} \sum_{i=1}^{n} \left\| \mathbf{x}_{i}^{0} - D_{\boldsymbol{\theta}}(\mathbf{x}_{i}^{t}, t, \mathbf{z}_{i}) \right\|_{2}^{2} + u_{\boldsymbol{\theta}}(t) \right], \tag{6}$$

where  $\mathbf{z}_i = F_{\phi}(\mathbf{v}_{\leq i}, \mathbf{x}_{< i}^0)$ , a loss weighting  $\lambda(t) = (t^2 + \sigma_{\text{data}}^2)/(t \cdot \sigma_{\text{data}})^2$ ,  $\ln t \sim \mathcal{N}(P_{\text{mean}}, P_{\text{std}})$ ,  $\sigma_{\text{data}}$  is the standard deviation of the training data, and  $u_{\theta}(t)$  is a one-layer MLP-based continuous uncertainty function quantifying the uncertainty for the denoising objective at noise level t (Karras et al., 2024). We provide the training algorithm of Stage 1 in Algorithm 1.

**Stage 2: Consistency fine-tuning via ECT** We further apply ECT to accelerate the diffusion head toward low per-frame latency. We minimize the following objective:

$$\mathcal{L}_{\text{Stage 2}}(\boldsymbol{\theta}, \boldsymbol{\phi}) = \mathbb{E}_{\mathbf{x}^0, t, r, \boldsymbol{\epsilon}} \left[ w(t) \sum_{i=1}^n d(G_{(\boldsymbol{\theta}, \boldsymbol{\phi})}(\mathbf{x}_i^t), G_{\text{sg}(\boldsymbol{\theta}, \boldsymbol{\phi})}(\mathbf{x}_i^r)) \right], \tag{7}$$

where  $G_{(\theta,\phi)}(\mathbf{x}_i^t) \triangleq G_{(\theta,\phi)}(\mathbf{x}_i^t, t, \mathbf{v}_{\leq i}, \mathbf{x}_{< i}^0)$  is the entire network (including diffusion head  $D_{\theta}$  and transformer  $F_{\phi}$ .). We initialize a model weight with the Stage 1 model. During training,  $\Delta t = t - r$  is gradually annealed as  $\Delta t \to 0$  by following a mapping function m(r|t, Iters) along with the number of training iterations Iters. We use m(r|t, Iters) formulated as:

$$m(r|t, \text{Iters}) = \left(1 - \frac{1}{q^{\lceil \text{Iters}/s \rceil}} k\sigma(-bt)\right) t,$$
 (8)

where  $\sigma(\cdot)$  is the sigmoid function, q, s, k, and b are hyperparameters that control the annealing schedule. Note that we finetune both the transformer and the diffusion head on Stage 2 (See an ablation on this in Appendix C.1.). We provide the training algorithm of Stage 2 in Algorithm 2.

### 3.4 Sampling Framework

At inference time, following the MAR decoding paradigm, we operate a two-stage procedure. First, we obtain  $\mathbf{z}_i$  by channel-wise concatenation  $\mathtt{Concat}(\tilde{\mathbf{z}}_{2i-1}, \tilde{\mathbf{z}}_{2i})$ , where  $\tilde{\mathbf{z}}_{2i-1}$  and  $\tilde{\mathbf{z}}_{2i}$  are outputs of the transformer. Second, the diffusion head samples  $\mathbf{x}_i^0$  conditioned on  $\mathbf{z}_i$  through the reverse-diffusion sampling with the Stage 1 model or CM sampling with the Stage 2 model.

To get  $\tilde{\mathbf{z}}_{2i}$  (a corresponding input token is a vision condition  $\mathbf{v}_i$ ), we apply Classifier-Free Guidance (CFG) (Ho & Salimans, 2022) on the transformer's sampling as  $\tilde{\mathbf{z}}_{2i} = \tilde{\mathbf{z}}_{2i}^{\text{null}} + \omega(\tilde{\mathbf{z}}_{2i}^{\text{cond}} - \tilde{\mathbf{z}}_{2i}^{\text{null}})$ , where  $\omega$  is a guidance scale,  $\tilde{\mathbf{z}}_{2i}^{\text{cond}}$  is the transformer output given the visual condition  $\mathbf{v}_i$ , and  $\tilde{\mathbf{z}}_{2i}^{\text{null}}$  is the output given a learnable null embedding, respectively. To get  $\tilde{\mathbf{z}}_{2i}^{\text{null}}$ , all the  $\mathbf{v}_{\leq i}$  are replaced with the learnable null embedding. To enable CFG sampling, we randomly replace all the video tokens  $\mathbf{v}_i(i=1,\ldots,n)$  by the null embedding during training. We use KV-cache (Shazeer, 2019) for efficient inference. We provide the sampling procedure in Algorithm 3. Since our CFG sampling scheme is not identical to the original MAR, we describe the difference in Appendix B.3 with an ablation study in Appendix C.2.

### 4 EXPERIMENTS

### 4.1 Dataset

Following the context of world models, we evaluate SoundReactor on the OGameData250K (Che et al., 2025) dataset, a large collection of gameplay videos from diverse AAA titles. From the original 250,000 videos (14-16 seconds each), we collected 230K available samples and manually filtered out clips containing only background music. This results in a training set of 94K samples (around 400 hours) and a test set of 3,830 samples. To ensure a balanced representation of each game, we create the train and test splits by maintaining a consistent clip ratio within each game title. All data is processed at 30 FPS with 480p resolution and 48 kHz stereo audio. During training, we randomly sample 8-second clips. Our primary evaluation is conducted on 8-second clips. We also test our models on longer sequence generation beyond the training context window on 16-second clips using zero-shot context-window extension techniques (Chen et al., 2023; Peng et al., 2024).

### 4.2 Comparing Methods

As discussed in the preceding sections, our scope is the frame-level online V2A task. To the best of our knowledge, no prior work explicitly addresses this setting. We therefore compare against offline AR V2A models, which are the most analogous to our setup. Specifically, we choose V-AURA (Viertola et al., 2025), as it achieves state-of-the-art performance in audio quality, audio-visual semantic alignment, and temporal synchronization among recent AR V2A models (Sheffer & Adi, 2023; Du et al., 2023; Mei et al., 2024b; Viertola et al., 2025).

**V-AURA** V-AURA employs a LLaMA-style architecture with Synchformer (lashin et al., 2024) as a video encoder and DAC (Kumar et al., 2023) as a discrete tokenizer. We train V-AURA on

325

326

327 328

335 336

337

338

344

345

346

347

348

349

350

351

352

353

354 355

356

357

358

359

360

361

362

363

364

365

366

367

368

369

370

371 372

373

374

375

376

377

Table 1: FAD and MMD on OGameData. Center is average over Left and Right channels. Diff is their difference. We retrained V-AURA. Note that V-AURA's video encoder extracts chunk-level features using non-causal self-attention across frames, so it is not strictly compatible with frame-level online V2A task. Bold and underlined scores indicate best and second-best results, respectively.

	Channels/				F	AD↓				MMD↓							
Model	Sample rate	OpenL3			LAION-CLAP		OpenL3				LAION-CLAP						
		Center	Diff	Left	Right	Center	Diff	Left	Right	Center	Diff	Left	Right	Center	Diff	Left	Right
Baselines																	
VAE-Reconstruction	2/48kHz	33.0	20.2	34.9	32.2	0.058	0.009	0.063	0.055	60.4	28.7	67.1	60.1	0.301	0.518	0.321	0.260
V-AURA† (Viertola et al., 2025)	1/44.1kHz	68.3	-	69.5	69.2	0.287	-	0.284	0.285	110	-	113	113	1.84	-	1.81	1.80
Proposed methods																	
SoundReactor-Diffusion	2/48kHz	36.8	25.7	40.1	37.8	0.139	0.257	0.159	0.155	67.6	37.2	77.6	71.5	0.702	1.52	0.828	0.787
SoundReactor-ECT (NFE=1)	2/48kHz	38.2	29.1	43.0	39.7	0.129	0.299	0.147	0.146	78.8	54.2	95.2	85.9	0.649	1.81	0.735	0.729
SoundReactor-ECT (NFE=2)	2/48kHz	35.1	24.8	39.5	36.1	0.105	0.250	0.121	0.115	70.0	43.1	85.0	74.9	0.509	1.47	0.595	0.549
SoundReactor-ECT (NFE=4)	2/48kHz	33.9	22.6	37.7	34.3	0.090	0.219	0.107	0.100	64.6	<u>35.4</u>	<u>77.1</u>	67.5	0.451	1.29	0.527	0.473

Table 2: FSAD, KL<sub>PaSST</sub>, IB-Score, and Table 3: Subjective evaluation on audio quality DeSync on OGameData. Bold score indicates the best results. We retrained V-AURA.

Model	$FSAD\downarrow$	$KL_{PaSST} \downarrow$	IB-Score ↑	DeSync↓
Baselines				
VAE-Reconstruction	0.00796	0.643	0.260	0.943
V-AURA† (Viertola et al., 2025)	0.113	1.96	0.223	0.982
Proposed methods				
SoundReactor-Diffusion	0.0219	1.61	0.292	1.06
SoundReactor-ECT (NFE=1)	0.0254	1.61	0.274	1.02
SoundReactor-ECT (NFE=2)	0.0206	1.60	0.277	1.01
SoundReactor-ECT (NFE=4)	0.0180	1.57	0.285	1.04

(Oval), semantic alignment (AV-Sem), temporal alignment (AV-Temp), and Stereo panning correctness (Stereo) with 95% Confidence Interval.

Model	Oval ↑	AV-Sem↑	AV-Temp ↑	Stereo ↑
Ground-truth	$83.6 \pm 2.44$	$82.2 \pm 2.71$	$83.4{\pm}2.52$	81.2±2.76
V-AURA† Ours-ECT (NFE=1) Ours-ECT (NFE=4)	42.2±3.93 61.9±3.07 <b>64.9</b> ± <b>3.01</b>	42.5±4.15 64.5±3.20 <b>65.2</b> ± <b>3.19</b>	50.5±4.07 58.4±3.55 <b>64.3</b> ± <b>3.53</b>	43.2±3.82 60.5±3.08 <b>65.3</b> ± <b>3.00</b>

offline V2A setups with OGameData250K by following the original training setups suggested by the authors. We retrain the transformer part. Crucially, although V-AURA's backbone is the AR transformer, its video encoder, Synchformer (Iashin et al., 2024), extracts chunk-level features using non-causal self-attention across frames (Iashin et al., 2024; Bertasius et al., 2021; Patrick et al., 2021) (i.e., Synchformer extracts chunks of video frames, and its video features contain future information), so it is not strictly compatible with the frame-level online V2A task<sup>5</sup>.

**SoundReactor** We evaluate two main variants of our model: SoundReactor-Diffusion (after Stage 1) and SoundReactor-ECT (after Stage 2). We also employ the reconstruction from our VAE as a reference. Unless otherwise specified, SoundReactor-Diffusion is sampled with a 30-step deterministic Heun solver (a Number of Function Evaluation (NFE)=59). We set  $\omega = 3.0$  to get  $\tilde{\mathbf{z}}_{2i}$  (See Section 3.4). We investigate the influence of  $\omega$  in Appendix C.2.

### 4.3 EVALUATION METRICS

**Audio quality** To evaluate audio quality, we use Frechet Audio Distance (FAD) (Gui et al., 2024), Maximum Mean Discrepancy (MMD) (Chung et al., 2025; Jayasumana et al., 2024), and Kullback-Leibler divergence based on PaSST (Koutini et al., 2022) (KL<sub>PaSST</sub>). For FAD and MMD, following prior work Evans et al. (2024; 2025); Gui et al. (2024), we use OpenL3 (Cramer et al., 2019) and LAION-CLAP (Wu\* et al., 2023) as audio feature extractors. Since our model is trained on stereo signals, we compute the metrics on four channel configurations: the left channel (Left), the right channel (Right), their average (Center), and their difference (Diff) (Steinmetz et al., 2021). We compute KL<sub>PaSST</sub> only on the Center. Furthermore, as a complementary metric to evaluate stereo quality, we also use Frechet Stereo Audio Distance (FSAD) (Sun et al., 2025), which is based on StereoCRW (Chen et al., 2022b) features.

**Audio-visual alignment** To evaluate audio-visual semantic and temporal alignment, we utilize ImageBind score (IB-Score) (Girdhar et al., 2023) and DeSync (Viertola et al., 2025) by following common practices (Cheng et al., 2025; Viertola et al., 2025). To compute DeSync, we take two crops (first 4.8 sec. and last 4.8 sec.) from the video and compute the average over the results (Cheng et al., 2025). We compute these two metrics only on the Center.

**Listening test** To complement our objective metrics, we conduct a subjective listening test following the MUSHRA style (ITU-R BS.1534-3). We compare three methods: V-AURA, SoundReactor-ECT (NFE=1), and SoundReactor-ECT (NFE=4). From a pool of 50 video clips, each of 17 human evaluators is presented with 10 randomly selected samples per method in addition to the ground truth as a hidden reference. Participants are asked to rate the generated audio based on four criteria on a

<sup>&</sup>lt;sup>5</sup>We note that their work targets the offline V2A task.

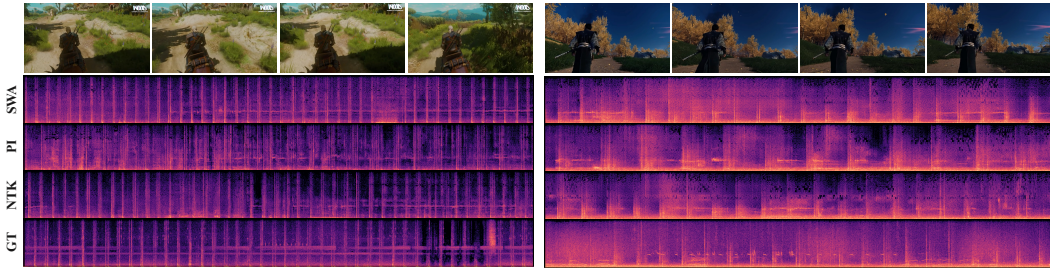


Figure 3: Spectrograms of long-seq. generation (twice the training window) with SoundReactor-ECT (NFE=4) comparing using Sliding Window Attention (SWA), Position Interpolation (PI), NTK-aware Interpolation (NTK) and the ground-truth (GT). PI results in a slower cadence for periodic sound.

scale of 0 to 100: overall audio quality (Oval), audio-visual semantic alignment (AV-Sem), temporal alignment (AV-Temp), and stereo quality and panning accuracy (Stereo). The evaluation interface is shown in Figure 9.

### 4.4 RESULTS

Effectiveness on frame-level online V2A generation The results of the quantitative and subjective evaluations are presented in Tables 1, 2, and 3. For these evaluations, V-AURA's monaural signal is duplicated for the left and right channels. Consequently, its Diff is omitted as the difference becomes zero. These tables show that our methods outperform V-AURA on all metrics except for DeSync, indicating the effectiveness of SoundReactor on the frame-level online V2A generation task. The results of FSAD in Table 2

Table 4: Performance on 16-sec. long-sequence generation, **evaluated on first and last** 8-sec. segments, independently. All methods generate the full 16-sec. sequence continuously, except for Baseline that generates two separate 8-sec.

36.0.1	First	8 sec.	Last 8 sec.			
Method	$FAD_{CLAP} \downarrow$	$MMD_{CLAP} \downarrow$	$FAD_{CLAP} \downarrow$	$\text{MMD}_{\text{CLAP}} \downarrow$		
Baseline Ours-ECT	0.116	0.466	0.115	0.477		
Long-seq. gen. Ours w/. SWA Ours w/. PI Ours w/. NTK	<b>0.111</b> 0.154 0.116	<b>0.461</b> 0.734 0.477	0.141 0.147 <b>0.111</b>	0.678 0.703 <b>0.459</b>		

and Stereo in Table 3 demonstrate that our model can generate stereo audio with panning accuracy with visual sound-event locations. We refer the generated audio samples to the demo page<sup>6</sup>. Comparing the performance of SoundReactor-Diffusion and ECTs in 1 to 3, the ECTs show comparable performance with the Diffusion even at NFE=1 on the head, and surpass it at NFE=4. While SoundReactor-Diffusion uses NFE=59, SoundReactor-ECTs require only 1~4 NFEs for the diffusion head, yielding 14.8× fewer NFEs at NFE=4 and 59× fewer at NFE=1, with a small performance degradation. We measure per-frame latency in wall-clock time in a later paragraph. As a supplementary evaluation, we benchmark our framework against various offline V2A approaches on the VGGSound dataset (Chen et al., 2020b) in Appendix C.4.

Generation beyond training context window We test our model on longer sequence generation beyond the training context window using zero-shot context-window extension techniques. Specifically, we use 16-second test set samples (1, 206 samples in total), which is twice the training context window. We apply and compare two common zero-shot RoPE scaling techniques to extend the context window: Position Interpolation (PI) (Chen et al., 2023) and NTK-aware interpolation (NTK) (Peng et al., 2024) (See Appendix B.4.) and Sliding Window Attention

Table 5: Overall performance on 16-sec. sequences. Features are extracted from 8-sec. sliding windows with a 1-sec. hop size. These features are then aggregated via mean-pooling to compute metrics.

Method	$FAD_{CLAP} \downarrow$	$\text{MMD}_{\text{CLAP}} \downarrow$		
Ours w/. SWA	0.108	0.475		
Ours w/. PI	0.138	0.668		
Ours w/. NTK	0.0992	0.412		

(SWA)<sup>7</sup> (Beltagy et al., 2020; Jiang et al., 2023). All the methods are applied on SoundReactor-ECT (NFE=4). Table 4 demonstrates that the NTK does not show significant performance degradation across either the first or last 8-second segment, despite extending the context window. In contrast, PI shows degradation throughout the entire sequence, while SWA degrades in the second half. This indicates that NTK-aware scaling effectively mitigates the distribution shift caused by long-sequence generation. In terms of overall quality, Table 5 shows that NTK and SWA are competitive, with

<sup>6</sup>https://anonymous-sr-submission.github.io/

<sup>&</sup>lt;sup>7</sup>Note that context window is not extended on SWA.

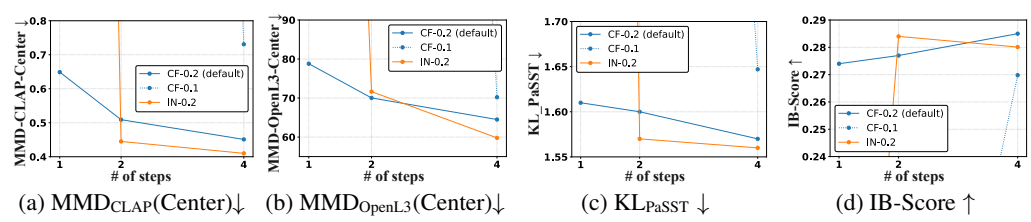


Figure 4: Ablation study on ECT. CF and IN indicate different mapping functions (see Appendix B.2). 0.1 and 0.2 denote dropout rates (Srivastava et al., 2014) during finetuning. CF-0.2 is our default.

PI performing worst. These results demonstrate that, by leveraging the NTK, our model achieves zero-shot context-window extrapolation without having the distribution shift. Given that interactive multimodal applications might require minute- to hour-scale generation, we leave exploring longer-horizon generation as future work. From qualitative observation, the spectrogram visualization in Figure 3 shows that PI slows periodic sounds (e.g., footsteps) and harms temporal synchronization, while NTK and SWA preserve timing (See Appendix B.4 for further discussion).

**Per-frame latency measurement** We measure two types of latency: wave-level and token-level latency. Wave-level latency is the elapsed time from feeding the previous audio token  $\mathbf{x}_{n-1}$  into the model until the output  $\mathbf{x}_n$  is incrementally decoded into a waveform, including the encoding of a raw video frame  $V_n$ . Token-level latency is identical to this but excludes the waveform decoding (Detailed in Appendix B.5). We perform this benchmark on a single H100 GPU with a batch size of one, using a single

Table 6: Mean and standard deviation of per-frame latencies over 50 clips. Lower than 33.3ms on wave-level latency is real-time operation.

Model (Ours-ECT)	Token-level latency [ms]↓	Wave-level latency [ms]↓
NFE=1	$26.6 \pm 2.93$	$32.4 \pm 1.91$
NFE=2	$27.4 \pm 2.60$	$34.7 \pm 2.13$
NFE=4	$30.3 \pm 2.41$	$38.6 \pm 1.46$

CUDA stream. We provide the mean and standard deviation over the 50 clips (30FPS, 480p, 16 second) with the default our ECT at  $\omega=3$ . As demonstrated in Table 6, while our model achieves remarkably low per-frame token-level latency, the overhead from incremental waveform decoding prevents the end-to-end wave-level latency from meeting the 33.3 ms target (real-time for 30FPS videos) except at NFE=1, which falls short of the generation quality of NFE=2 and 4. Addressing this bottleneck to enable real-time high-quality generation for practical applications remains an important direction for future work.

# 4.5 ABLATION STUDY

Here, we ablate two factors in ECT that crucially affect sample quality: i) the mapping function in Eq (8) and ii) the network dropout rate (Srivastava et al., 2014). We use two representative choices from Geng et al. (2025b), denoted IN and CF (detailed in Appendix B.2). Under CF, we test dropout rates of 0.1 and 0.2 (CF-0.2 is identical to our default ECT.). As shown in Figure 4, comparing CF-0.1 and CF-0.2 reveals that the dropout rate substantially impacts sample quality. This aligns with prior findings in Song & Dhariwal (2024); Geng et al. (2025b) and newly shows that tuning it remains significantly important even in MAR-style models. Comparing IN-0.2 and CF-0.2, both settings show comparable performance on NFE=2 and 4. Notably, however, only CF-0.2 can generate high-quality samples with NFE=1. For a deeper understanding of our model, we provide extensive ablations on various aspects of both the generator (in Appendix C.1 and C.2) and vision conditioning (in Appendix C.3), which demonstrate that our design choices contribute to the overall performance.

### 5 CONCLUSION

In this work, we introduce the novel task of frame-level online V2A generation and propose SoundReactor, the first simple yet effective framework tailored for this setting. Our experiments demonstrate that SoundReactor achieves high-quality full-band stereo audio generation under the end-to-end causal constraint while maintaining low per-frame token-level latency. Extensive ablations provide key insights into the respective contributions of our design choices within our framework. We anticipate this work will motivate the research community on sound generative models to explore interactive multimodal applications, providing a foundational component for live content creation and sounding world models.

# **ETHICS STATEMENT**

SoundReactor poses a risk for generating harmful or inappropriate content, offensive sound effects, or even sound content that infringes on copyrights. To mitigate these risks, it is crucial to carefully curate the training data as a first step. Furthermore, addressing these risks involves implementing robust content filtering, moderation mechanisms to prevent the creation of unethical, harmful content.

### REPRODUCIBILITY STATEMENT

The source code is available at the submitted supplementary materials, and the checkpoints are available at <a href="https://drive.google.com/drive/folders/1AVfogi4nxKlVesDi-LP4migAuN8C3jp7?usp=sharing">https://drive.google.com/drive/folders/1AVfogi4nxKlVesDi-LP4migAuN8C3jp7?usp=sharing</a>. Moreover, we outline our training and sampling procedures in Algorithm 1, Algorithm 2, and Algorithm 3, and detailed implementation instructions for result reproducibility can be found in Appendix B.1. After acceptance, we will open-source our codebase.

# THE USE OF LARGE LANGUAGE MODELS

We utilized LLMs for academic proofreading and finding related work. We also used them for coding assistance and visualization of experimental results. However, all research ideas were developed solely by the authors.

# REFERENCES

- Yatong Bai, Trung Dang, Dung Tran, Kazuhito Koishida, and Somayeh Sojoudi. Consistencytta: Accelerating diffusion-based text-to-audio generation with consistency distillation. In *INTER-SPEECH*, 2024.
- Federico Baldassarre, Marc Szafraniec, Basile Terver, Vasil Khalidov, Francisco Massa, Yann LeCun, Patrick Labatut, Maximilian Seitzer, and Piotr Bojanowski. Back to the features: Dino as a foundation for video world models. *arXiv preprint arXiv:2507.19468*, 2025. URL https://arxiv.org/abs/2507.19468.
- Philip J. Ball, Jakob Bauer, Frank Belletti, Bethanie Brownfield, Ariel Ephrat, Shlomi Fruchter, Agrim Gupta, Kristian Holsheimer, Aleksander Holynski, Jiri Hron, Christos Kaplanis, Marjorie Limont, Matt McGill, Yanko Oliveira, Jack Parker-Holder, Frank Perbet, Guy Scully, Jeremy Shar, Stephen Spencer, Omer Tov, Ruben Villegas, Emma Wang, Jessica Yung, Cip Baetu, Jordi Berbel, David Bridson, Jake Bruce, Gavin Buttimore, Sarah Chakera, Bilva Chandra, Paul Collins, Alex Cullum, Bogdan Damoc, Vibha Dasagi, Maxime Gazeau, Charles Gbadamosi, Woohyun Han, Ed Hirst, Ashyana Kachra, Lucie Kerley, Kristian Kjems, Eva Knoepfel, Vika Koriakin, Jessica Lo, Cong Lu, Zeb Mehring, Alex Moufarek, Henna Nandwani, Valeria Oliveira, Fabio Pardo, Jane Park, Andrew Pierson, Ben Poole, Helen Ran, Tim Salimans, Manuel Sanchez, Igor Saprykin, Amy Shen, Sailesh Sidhwani, Duncan Smith, Joe Stanton, Hamish Tomlinson, Dimple Vijaykumar, Luyu Wang, Piers Wingfield, Nat Wong, Keyang Xu, Christopher Yew, Nick Young, Vadim Zubov, Douglas Eck, Dumitru Erhan, Koray Kavukcuoglu, Demis Hassabis, Zoubin Gharamani, Raia Hadsell, Aäron van den Oord, Inbar Mosseri, Adrian Bolton, Satinder Singh, and Tim Rocktäschel. Genie 3: A new frontier for world models, 2025. URL https://deepmind.google/discover/blog/genie-3-a-new-frontier-for-world-models/.
- Iz Beltagy, Matthew E. Peters, and Arman Cohan. Longformer: The long-document transformer. arXiv preprint arXiv:2004.05150, 2020. URL https://arxiv.org/abs/2004.05150.
- Roi Benita, Michael Finkelson, Tavi Halperin, Gleb Sterkin, and Yossi Adi. Controllable automatic foley artist. In *Proc. IEEE International Conference on Computer Vision (ICCV)*, 2025.
- Gedas Bertasius, Heng Wang, and Lorenzo Torresani. Is space-time attention all you need for video understanding? In *Proc. International Conference on Machine Learning (ICML)*, 2021.
- Jake Bruce, Michael D Dennis, Ashley Edwards, Jack Parker-Holder, Yuge Shi, Edward Hughes, Matthew Lai, Aditi Mavalankar, Richie Steigerwald, Chris Apps, Yusuf Aytar, Sarah Maria Elisabeth Bechtle, Feryal Behbahani, Stephanie C.Y. Chan, Nicolas Heess, Lucy Gonzalez, Simon Osindero, Sherjil Ozair, Scott Reed, Jingwei Zhang, Konrad Zolna, Jeff Clune, Nando de Freitas, Satinder Singh, and Tim Rocktäschel. Genie: Generative interactive environments. In *Proc. International Conference on Machine Learning (ICML)*, 2024. URL https://openreview.net/forum?id=bJbSbJskOS.
- Huiwen Chang, Han Zhang, Lu Jiang, Ce Liu, and William T. Freeman. Maskgit: Masked generative image transformer. In *Proc. IEEE Conference on Computer Vision and Pattern Recognition (CVPR)*, pp. 11305–11315, 2022.
- Haoxuan Che, Xuanhua He, Quande Liu, Cheng Jin, and Hao Chen. Gamegen-x: Interactive openworld game video generation. In *Proc. International Conference on Learning Representation (ICLR)*, 2025. URL https://openreview.net/forum?id=8VG8tpPZhe.
- Changan Chen, Unnat Jain, Carl Schissler, Sebastia Vicenc Amengual Gari, Ziad Al-Halah, Vamsi Krishna Ithapu, Philip Robinson, and Kristen Grauman. Soundspaces: Audio-visual navigaton in 3d environments. In *Proc. European Conference on Computer Vision (ECCV)*, 2020a.
- Changan Chen, Carl Schissler, Sanchit Garg, Philip Kobernik, Alexander Clegg, Paul Calamia, Dhruv Batra, Philip W Robinson, and Kristen Grauman. Soundspaces 2.0: A simulation platform for visual-acoustic learning. In *Proc. Advances in Neural Information Processing Systems (NeurIPS)*, 2022a.
- Honglie Chen, Weidi Xie, Andrea Vedaldi, and Andrew Zisserman. Vggsound: A large-scale audiovisual dataset. In *Proc. IEEE Int. Conf. Acoust., Speech, Signal Process. (ICASSP)*, 2020b.

- Shouyuan Chen, Sherman Wong, Liangjian Chen, and Yuandong Tian. Extending context window of large language models via positional interpolation. *arXiv* preprint arXiv:2306.15595, 2023. URL https://arxiv.org/abs/2306.15595.
- Ziyang Chen, David F Fouhey, and Andrew Owens. Sound localization by self-supervised time delay estimation. In *Proc. European Conference on Computer Vision (ECCV)*, 2022b.
- Ziyang Chen, Prem Seetharaman, Bryan Russell, Oriol Nieto, David Bourgin, Andrew Owens, and Justin Salamon. Video-guided foley sound generation with multimodal controls. In *Proc. IEEE Conference on Computer Vision and Pattern Recognition (CVPR)*, 2025.
- Ho Kei Cheng, Masato Ishii, Akio Hayakawa, Takashi Shibuya, Alexander Schwing, and Yuki Mitsufuji. MMAudio: Taming multimodal joint training for high-quality video-to-audio synthesis. In *Proc. IEEE Conference on Computer Vision and Pattern Recognition (CVPR)*, 2025.
- Yoonjin Chung, Pilsun Eu, Junwon Lee, Keunwoo Choi, Juhan Nam, and Ben Sangbae Chon. Kad: No more fad! an effective and efficient evaluation metric for audio generation. *arXiv* preprint *arXiv*:2502.15602, 2025. URL https://arxiv.org/abs/2502.15602.
- Marco Comunità, Zhi Zhong, Akira Takahashi, Shiqi Yang, Mengjie Zhao, Koichi Saito, Yukara Ikemiya, Takashi Shibuya, Shusuke Takahashi, and Yuki Mitsufuji. Specmaskgit: Masked generative modeling of audio spectrogram for efficient audio synthesis and beyond. In *Proc. Int. Society for Music Information Retrieval Conf. (ISMIR)*, 2024.
- Jade Copet, Felix Kreuk, Itai Gat, Tal Remez, David Kant, Gabriel Synnaeve, Yossi Adi, and Alexandre Defossez. Simple and controllable music generation. In A. Oh, T. Naumann, A. Globerson, K. Saenko, M. Hardt, and S. Levine (eds.), *Proc. Advances in Neural Information Processing Systems (NeurIPS)*, volume 36, pp. 47704–47720. Curran Associates, Inc., 2023. URL https://proceedings.neurips.cc/paper\_files/paper/2023/file/94b472a1842cd7c56dcb125fb2765fbd-Paper-Conference.pdf.
- Aurora Linh Cramer, Ho-Hsiang Wu, Justin Salamon, and Juan Pablo Bello. Look, listen, and learn more: Design choices for deep audio embeddings. In *Proc. IEEE Int. Conf. Acoust., Speech, Signal Process. (ICASSP)*, pp. 3852–3856, 2019.
- Tri Dao. FlashAttention-2: Faster attention with better parallelism and work partitioning. In *Proc. International Conference on Learning Representation (ICLR)*, 2024.
- Alexandre Défossez, Jade Copet, Gabriel Synnaeve, and Yossi Adi. High fidelity neural audio compression. *Transactions on Machine Learning Research*, 2023. ISSN 2835-8856. URL https://openreview.net/forum?id=ivCd8z8zR2. Featured Certification, Reproducibility Certification.
- Alexandre Défossez, Laurent Mazaré, Manu Orsini, Amélie Royer, Patrick Pérez, Hervé Jégou, Edouard Grave, and Neil Zeghidour. Moshi: a speech-text foundation model for real-time dialogue. arXiv preprint arXiv:2410.00037, 2024. URL https://arxiv.org/abs/2410.00037.
- Yuexi Du, Ziyang Chen, Justin Salamon, Bryan Russell, and Andrew Owens. Conditional generation of audio from video via foley analogies. In *Proc. IEEE Conference on Computer Vision and Pattern Recognition (CVPR)*, 2023.
- Bradley Efron. Tweedie's formula and selection bias. *Journal of the American Statistical Association*, 106:1602 1614, 2011.
- Patrick Esser, Sumith Kulal, Andreas Blattmann, Rahim Entezari, Jonas Müller, Harry Saini, Yam Levi, Dominik Lorenz, Axel Sauer, Frederic Boesel, Dustin Podell, Tim Dockhorn, Zion English, Kyle Lacey, Alex Goodwin, Yannik Marek, and Robin Rombach. Scaling rectified flow transformers for high-resolution image synthesis. In *Proc. International Conference on Machine Learning (ICML)*, 2024.
- Zach Evans, CJ Carr, Josiah Taylor, Scott H. Hawley, and Jordi Pons. Fast timing-conditioned latent audio diffusion. *Proc. International Conference on Machine Learning (ICML)*, 2024.

- Zach Evans, Julian D. Parker, CJ Carr, Zack Zukowski, Josiah Taylor, and Jordi Pons. Stable audio open. In *Proc. IEEE Int. Conf. Acoust., Speech, Signal Process. (ICASSP)*, pp. 1–5, 2025.
  - Zhengyang Geng, Mingyang Deng, Xingjian Bai, J. Zico Kolter, and Kaiming He. Mean flows for one-step generative modeling. *arxiv preprint arXiv:2505.13447*, 2025a. URL https://arxiv.org/abs/2505.13447.
  - Zhengyang Geng, Ashwini Pokle, Weijian Luo, Justin Lin, and J Zico Kolter. Consistency models made easy. In *Proc. International Conference on Learning Representation (ICLR)*, 2025b. URL https://openreview.net/forum?id=xQVxo9dSID.
  - Rohit Girdhar, Alaaeldin El-Nouby, Zhuang Liu, Mannat Singh, Kalyan Vasudev Alwala, Armand Joulin, and Ishan Misra. Imagebind: One embedding space to bind them all. In *Proc. IEEE Conference on Computer Vision and Pattern Recognition (CVPR)*, 2023.
  - Azalea Gui, Hannes Gamper, Sebastian Braun, and Dimitra Emmanouilidou. Adapting frechet audio distance for generative music evaluation. In *Proc. IEEE Int. Conf. Acoust., Speech, Signal Process.* (*ICASSP*), pp. 1331–1335, 2024.
  - David Ha and Jürgen Schmidhuber. Recurrent world models facilitate policy evolution. In *Proc. Advances in Neural Information Processing Systems (NeurIPS)*, volume 31, 2018. URL https://proceedings.neurips.cc/paper\_files/paper/2018/file/2de5d16682c3c35007e4e92982fla2ba-Paper.pdf.
  - Kaiming He, Xiangyu Zhang, Shaoqing Ren, and Jian Sun. Deep residual learning for image recognition. In *Proc. IEEE Conference on Computer Vision and Pattern Recognition (CVPR)*, pp. 770–778, 2016.
  - Xianglong He, Chunli Peng, Zexiang Liu, Boyang Wang, Yifan Zhang, Qi Cui, Fei Kang, Biao Jiang, Mengyin An, Yangyang Ren, Baixin Xu, Hao-Xiang Guo, Kaixiong Gong, Xuchen Song, Yang Liu, Eric Li, and Yahui Zhou. Matrix-game 2.0: An open-source, real-time, and streaming interactive world model, 2025. URL https://matrix-game-v2.github.io/static/pdf/report.pdf.
  - Jonathan Ho and Tim Salimans. Classifier-free diffusion guidance. *In arXiv e-prints: 2207.12598*, 2022.
  - Jonathan Ho, Ajay Jain, and Pieter Abbeel. Denoising diffusion probabilistic models. In *Proc. Advances in Neural Information Processing Systems (NeurIPS)*, volume 33, pp. 6840–6851, 2020.
  - Vladimir Iashin and Esa Rahtu. Taming visually guided sound generation. In *British Machine Vision Conference (BMVC)*, 2021.
  - Vladimir Iashin, Weidi Xie, Esa Rahtu, and Andrew Zisserman. Sparse in space and time: Audiovisual synchronisation with trainable selectors. In 33rd British Machine Vision Conference 2022, BMVC 2022, London, UK, November 21-24, 2022. BMVA Press, 2022.
  - Vladimir Iashin, Weidi Xie, Esa Rahtu, and Andrew Zisserman. Synchformer: Efficient synchronization from sparse cues. In *Proc. IEEE Int. Conf. Acoust., Speech, Signal Process. (ICASSP)*, 2024.
  - Sadeep Jayasumana, Srikumar Ramalingam, Andreas Veit, Daniel Glasner, Ayan Chakrabarti, and Sanjiv Kumar. Rethinking fid: Towards a better evaluation metric for image generation. In *Proc. IEEE Conference on Computer Vision and Pattern Recognition (CVPR)*, 2024.
  - Yujin Jeong, Yunji Kim, Sanghyuk Chun, and Jiyoung Lee. Read, watch and scream! sound generation from text and video. In *Proc. AAAI Conference on Artificial Intelligence (AAAI)*, 2024.
  - Dongya Jia, Zhuo Chen, Jiawei Chen, Chenpeng Du, Jian Wu, Jian Cong, Xiaobin Zhuang, Chumin Li, Zhen Wei, Yuping Wang, and Yuxuan Wang. DiTAR: Diffusion transformer autoregressive modeling for speech generation. In *Proc. International Conference on Machine Learning (ICML)*, 2025. URL https://openreview.net/forum?id=8tRtweTTwv.

- Albert Q. Jiang, Alexandre Sablayrolles, Arthur Mensch, Chris Bamford, Devendra Singh Chaplot, Diego de las Casas, Florian Bressand, Gianna Lengyel, Guillaume Lample, Lucile Saulnier, Lélio Renard Lavaud, Marie-Anne Lachaux, Pierre Stock, Teven Le Scao, Thibaut Lavril, Thomas Wang, Timothée Lacroix, and William El Sayed. Mistral 7b. *arXiv preprint arXiv:2310.06825*, 2023. URL https://arxiv.org/abs/2310.06825.
- Ian Jolliffe. *Principal Component Analysis*, pp. 1094–1096. Springer Berlin Heidelberg, Berlin, Heidelberg, 2011. ISBN 978-3-642-04898-2. doi: 10.1007/978-3-642-04898-2\_455. URL https://doi.org/10.1007/978-3-642-04898-2\_455.
- Tero Karras, Miika Aittala, Timo Aila, and Samuli Laine. Elucidating the design space of diffusion-based generative models. In *Proc. Advances in Neural Information Processing Systems (NeurIPS)*, 2022.
- Tero Karras, Miika Aittala, Jaakko Lehtinen, Janne Hellsten, Timo Aila, and Samuli Laine. Analyzing and improving the training dynamics of diffusion models. In *Proc. IEEE Conference on Computer Vision and Pattern Recognition (CVPR)*, 2024.
- Dongjun Kim, Chieh-Hsin Lai, Wei-Hsiang Liao, Naoki Murata, Yuhta Takida, Toshimitsu Uesaka, Yutong He, Yuki Mitsufuji, and Stefano Ermon. Consistency trajectory models: Learning probability flow ode trajectory of diffusion. In *Proc. International Conference on Learning Representation (ICLR)*, 2024.
- Diederik P Kingma and Max Welling. Auto-encoding variational bayes. In *Proc. International Conference on Learning Representation (ICLR)*, 2014.
- Khaled Koutini, Jan Schlüter, Hamid Eghbal-zadeh, and Gerhard Widmer. Efficient training of audio transformers with patchout. In *INTERSPEECH*, pp. 2753–2757, 2022.
- Rithesh Kumar, Prem Seetharaman, Alejandro Luebs, Ishaan Kumar, and Kundan Kumar. High-fidelity audio compression with improved rvqgan. In *Proc. Advances in Neural Information Processing Systems (NeurIPS)*, 2023.
- Gael Le Lan, Bowen Shi, Zhaoheng Ni, Sidd Srinivasan, Anurag Kumar, Brian Ellis, David Kant, Varun K. Nagaraja, Ernie Chang, Wei-Ning Hsu, Yangyang Shi, and Vikas Chandra. High fidelity text-guided music editing via single-stage flow matching. In *Audio Imagination: NeurIPS 2024 Workshop AI-Driven Speech, Music, and Sound Generation*, 2024. URL https://openreview.net/forum?id=PhJstgkZxJ.
- Jiaqi Li, Junshu Tang, Zhiyong Xu, Longhuang Wu, Yuan Zhou, Shuai Shao, Tianbao Yu, Zhiguo Cao, and Qinglin Lu. Hunyuan-gamecraft: High-dynamic interactive game video generation with hybrid history condition, 2025a. URL https://arxiv.org/abs/2506.17201.
- Tianhong Li, Yonglong Tian, He Li, Mingyang Deng, and Kaiming He. Autoregressive image generation without vector quantization. In *Proc. Advances in Neural Information Processing Systems (NeurIPS)*, 2024. URL https://openreview.net/forum?id=VNBIF0gmkb.
- Yunpeng Li, Kehang Han, Brian McWilliams, Zalan Borsos, and Marco Tagliasacchi. Spectrostream: A versatile neural codec for general audio. *arxiv preprint arXiv:2508.05207*, 2025b. URL https://arxiv.org/abs/2508.05207.
- Haohe Liu, Zehua Chen, Yi Yuan, Xinhao Mei, Xubo Liu, Danilo Mandic, Wenwu Wang, and Mark D Plumbley. AudioLDM: Text-to-audio generation with latent diffusion models. In *Proc. International Conference on Machine Learning (ICML)*, pp. 21450–21474, 2023a.
- Huadai Liu, Jialei Wang, Kaicheng Luo, Wen Wang, Qian Chen, Zhou Zhao, and Wei Xue. Thinksound: Chain-of-thought reasoning in multimodal large language models for audio generation and editing. In *Proc. Advances in Neural Information Processing Systems (NeurIPS)*, 2025.
- Xingchao Liu, Chengyue Gong, and Qiang Liu. Flow straight and fast: Learning to generate and transfer data with rectified flow. In *Proc. International Conference on Learning Representation (ICLR)*, 2023b.

- Xiulong Liu, Kun Su, and Eli Shlizerman. Tell what you hear from what you see–video to audio generation through text. In *Proc. Advances in Neural Information Processing Systems (NeurIPS)*, 2024a.
  - Zeyi Liu, Cheng Chi, Eric Cousineau, Naveen Kuppuswamy, Benjamin Burchfiel, and Shuran Song. Maniwav: Learning robot manipulation from in-the-wild audio-visual data. *arXiv preprint arXiv:2406.19464*, 2024b.
  - Ilya Loshchilov and Frank Hutter. Decoupled Weight Decay Regularization. In *Proc. International Conference on Learning Representation (ICLR)*, 2019.
  - Cheng Lu and Yang Song. Simplifying, stabilizing and scaling continuous-time consistency models. In *Proc. International Conference on Learning Representation (ICLR)*, 2025. URL https://openreview.net/forum?id=LyJi5ugyJx.
  - Simian Luo, Chuanhao Yan, Chenxu Hu, and Hang Zhao. Diff-foley: Synchronized video-to-audio synthesis with latent diffusion models. In *Proc. Advances in Neural Information Processing Systems (NeurIPS)*, 2023. URL https://openreview.net/forum?id=q5FAZAIooz.
  - Xinhao Mei, Chutong Meng, Haohe Liu, Qiuqiang Kong, Tom Ko, Chengqi Zhao, Mark D. Plumbley, Yuexian Zou, and Wenwu Wang. Wavcaps: A chatgpt-assisted weakly-labelled audio captioning dataset for audio-language multimodal research. *IEEE/ACM Trans. Audio, Speech and Lang. Proc.*, 32:3339–3354, June 2024a. ISSN 2329-9290. doi: 10.1109/TASLP.2024.3419446. URL https://doi.org/10.1109/TASLP.2024.3419446.
  - Xinhao Mei, Varun Nagaraja, Gael Le Lan, Zhaoheng Ni, Ernie Chang, Yangyang Shi, and Vikas Chandra. Foleygen: Visually-guided audio generation. In 2024 IEEE 34th International Workshop on Machine Learning for Signal Processing (MLSP), pp. 1–6, 2024b.
  - Lingwei Meng, Long Zhou, Shujie Liu, Sanyuan Chen, Bing Han, Shujie Hu, Yanqing Liu, Jinyu Li, Sheng Zhao, Xixin Wu, Helen M. Meng, and Furu Wei. Autoregressive speech synthesis without vector quantization. In *Proceedings of the 63rd Annual Meeting of the Association for Computational Linguistics (Volume 1: Long Papers)*, pp. 1287–1300, 2025. URL https://aclanthology.org/2025.acl-long.65/.
  - Microsoft. Whamm! real-time world modelling of interactive environments, 2025. URL https://www.microsoft.com/en-us/research/articles/whamm-real-time-world-modelling-of-interactive-environments/.
  - Zachary Novack, Zach Evans, Zack Zukowski, Josiah Taylor, CJ Carr, Julian Parker, Adnan Al-Sinan, Gian Marco Iodice, Julian McAuley, Taylor Berg-Kirkpatrick, and Jordi Pons. Fast text-to-audio generation with adversarial post-training. In *Proc. IEEE Int. Workshop Appl. Signal Process. Audio Acoust. (WASPAA)*, 2025a.
  - Zachary Novack, Ge Zhu, Jonah Casebeer, Julian McAuley, Taylor Berg-Kirkpatrick, and Nicholas J. Bryan. Presto! distilling steps and layers for accelerating music generation. In *Proc. International Conference on Learning Representation (ICLR)*, 2025b. URL https://openreview.net/forum?id=Gj5JTAwdoy.
  - NVIDIA, :, Niket Agarwal, Arslan Ali, Maciej Bala, Yogesh Balaji, Erik Barker, Tiffany Cai, Prithvijit Chattopadhyay, Yongxin Chen, Yin Cui, Yifan Ding, Daniel Dworakowski, Jiaojiao Fan, Michele Fenzi, Francesco Ferroni, Sanja Fidler, Dieter Fox, Songwei Ge, Yunhao Ge, Jinwei Gu, Siddharth Gururani, Ethan He, Jiahui Huang, Jacob Huffman, Pooya Jannaty, Jingyi Jin, Seung Wook Kim, Gergely Klár, Grace Lam, Shiyi Lan, Laura Leal-Taixe, Anqi Li, Zhaoshuo Li, Chen-Hsuan Lin, Tsung-Yi Lin, Huan Ling, Ming-Yu Liu, Xian Liu, Alice Luo, Qianli Ma, Hanzi Mao, Kaichun Mo, Arsalan Mousavian, Seungjun Nah, Sriharsha Niverty, David Page, Despoina Paschalidou, Zeeshan Patel, Lindsey Pavao, Morteza Ramezanali, Fitsum Reda, Xiaowei Ren, Vasanth Rao Naik Sabavat, Ed Schmerling, Stella Shi, Bartosz Stefaniak, Shitao Tang, Lyne Tchapmi, Przemek Tredak, Wei-Cheng Tseng, Jibin Varghese, Hao Wang, Haoxiang Wang, Heng Wang, Ting-Chun Wang, Fangyin Wei, Xinyue Wei, Jay Zhangjie Wu, Jiashu Xu, Wei Yang, Lin Yen-Chen, Xiaohui Zeng, Yu Zeng, Jing Zhang, Qinsheng Zhang, Yuxuan Zhang, Qingqing Zhao, and Artur Zolkowski. Cosmos world foundation model platform for physical ai. arxiv preprint arXiv:2501.03575, 2025. URL https://arxiv.org/abs/2501.03575.

- Maxime Oquab, Timothée Darcet, Théo Moutakanni, Huy V. Vo, Marc Szafraniec, Vasil Khalidov, Pierre Fernandez, Daniel HAZIZA, Francisco Massa, Alaaeldin El-Nouby, Mido Assran, Nicolas Ballas, Wojciech Galuba, Russell Howes, Po-Yao Huang, Shang-Wen Li, Ishan Misra, Michael Rabbat, Vasu Sharma, Gabriel Synnaeve, Hu Xu, Herve Jegou, Julien Mairal, Patrick Labatut, Armand Joulin, and Piotr Bojanowski. DINOv2: Learning robust visual features without supervision. *Transactions on Machine Learning Research*, 2024. ISSN 2835-8856. URL https://openreview.net/forum?id=a68SUt6zFt. Featured Certification.
- Santiago Pascual, Chunghsin Yeh, Ioannis Tsiamas, and Joan Serrà. Masked generative video-to-audio transformers with enhanced synchronicity. In *Proc. European Conference on Computer Vision (ECCV)*, 2024.
- Marco Pasini, Javier Nistal, Stefan Lattner, and George Fazekas. Continuous autoregressive models with noise augmentation avoid error accumulation. *arXiv preprint arXiv:2411.18447*, 2024. URL https://arxiv.org/abs/2411.18447.
- Mandela Patrick, Dylan Campbell, Yuki M. Asano, Ishan Misra Florian Metze, Christoph Feichtenhofer, Andrea Vedaldi, and Joao F. Henriques. Keeping your eye on the ball: Trajectory attention in video transformers. In *Proc. Advances in Neural Information Processing Systems (NeurIPS)*, 2021.
- Bowen Peng, Jeffrey Quesnelle, Honglu Fan, and Enrico Shippole. YaRN: Efficient context window extension of large language models. In *Proc. International Conference on Learning Representation (ICLR)*, 2024. URL https://openreview.net/forum?id=wHBfxhZulu.
- Alec Radford, Jong Wook Kim, Chris Hallacy, Aditya Ramesh, Gabriel Goh, Sandhini Agarwal, Girish Sastry, Amanda Askell, Pamela Mishkin, Jack Clark, Gretchen Krueger, and Ilya Sutskever. Learning transferable visual models from natural language supervision. In *Proc. International Conference on Machine Learning (ICML)*, 2021.
- Mike Ranzinger, Greg Heinrich, Jan Kautz, and Pavlo Molchanov. Am-radio: Agglomerative vision foundation model reduce all domains into one. In *Proc. IEEE Conference on Computer Vision and Pattern Recognition (CVPR)*, pp. 12490–12500, 2024. doi: 10.1109/CVPR52733.2024.01187.
- Simon Rouard, Manu Orsini, Axel Roebel, Neil Zeghidour, and Alexandre Défossez. Continuous audio language models. *arXiv preprint arXiv:2509.06926*, 2025. URL https://arxiv.org/abs/2509.06926.
- Koichi Saito, Dongjun Kim, Takashi Shibuya, Chieh-Hsin Lai, Zhi Zhong, Yuhta Takida, and Yuki Mitsufuji. SoundCTM: Unifying score-based and consistency models for full-band text-to-sound generation. In *Proc. International Conference on Learning Representation (ICLR)*, 2025. URL https://openreview.net/forum?id=KrK6zXbjf0.
- Jürgen Schmidhuber. Making the world differentiable: on using self supervised fully recurrent neural networks for dynamic reinforcement learning and planning in non-stationary environments. Forschungsberichte Künstliche Intelligenz. Inst. für Informatik, 1990. URL https://books.google.com/books?id=9c2shaaacaaj.
- Noam Shazeer. Fast transformer decoding: One write-head is all you need. *arXiv preprint arXiv:1911.02150*, 2019. URL https://arxiv.org/abs/1911.02150.
- Noam Shazeer. Glu variants improve transformer. *arxiv preprint arXiv:2002.05202*, 2020. URL https://arxiv.org/abs/2002.05202.
- Roy Sheffer and Yossi Adi. I hear your true colors: Image guided audio generation. In *Proc. IEEE Int. Conf. Acoust., Speech, Signal Process. (ICASSP)*, 2023.
- Yang Song and Prafulla Dhariwal. Improved techniques for training consistency models. In *Proc. International Conference on Learning Representation (ICLR)*, 2024. URL https://openreview.net/forum?id=WNzy9bRDvG.
- Yang Song, Jascha Sohl-Dickstein, Diederik P. Kingma, Abhishek Kumar, Stefano Ermon, and Ben Poole. Score-based generative modeling through stochastic differential equations. In *Proc. International Conference on Learning Representation (ICLR)*, 2021.

Yang Song, Prafulla Dhariwal, Mark Chen, and Ilya Sutskever. Consistency models. *Proc. International Conference on Machine Learning (ICML)*, 2023.

- Nitish Srivastava, Geoffrey Hinton, Alex Krizhevsky, Ilya Sutskever, and Ruslan Salakhutdinov. Dropout: a simple way to prevent neural networks from overfitting. *The journal of machine learning research*, 15(1):1929–1958, 2014.
- Christian J. Steinmetz, Jordi Pons, Santiago Pascual, and Joan Serrà. Automatic multitrack mixing with a differentiable mixing console of neural audio effects. In *Proc. IEEE Int. Conf. Acoust.*, *Speech, Signal Process. (ICASSP)*, pp. 71–75, 2021. doi: 10.1109/ICASSP39728.2021.9414364.
- Jianlin Su, Murtadha Ahmed, Yu Lu, Shengfeng Pan, Wen Bo, and Yunfeng Liu. Roformer: Enhanced transformer with rotary position embedding. *Neurocomput.*, 568(C), February 2024. ISSN 0925-2312. doi: 10.1016/j.neucom.2023.127063. URL https://doi.org/10.1016/j.neucom.2023.127063.
- Peiwen Sun, Sitong Cheng, Xiangtai Li, Zhen Ye, Huadai Liu, Honggang Zhang, Wei Xue, and Yike Guo. Both ears wide open: Towards language-driven spatial audio generation. In *Proc. International Conference on Learning Representation (ICLR)*, 2025. URL https://openreview.net/forum?id=qPx3i9sMxv.
- Matthew Tancik, Pratul Srinivasan, Ben Mildenhall, Sara Fridovich-Keil, Nithin Raghavan, Utkarsh Singhal, Ravi Ramamoorthi, Jonathan Barron, and Ren Ng. Fourier features let networks learn high frequency functions in low dimensional domains. In H. Larochelle, M. Ranzato, R. Hadsell, M.F. Balcan, and H. Lin (eds.), *Proc. Advances in Neural Information Processing Systems (NeurIPS)*, volume 33, pp. 7537–7547. Curran Associates, Inc., 2020. URL https://proceedings.neurips.cc/paper\_files/paper/2020/file/55053683268957697aa39fba6f231c68-Paper.pdf.
- Google DeepMind Open-Ended Learning Team. Generally capable agents emerge from open-ended play, 2021. URL https://deepmind.google/discover/blog/generally-capable-agents-emerge-from-open-ended-play/.
- Google DeepMind SIMA Team. A generalist ai agent for 3d virtual environments, 2024. URL https://deepmind.google/discover/blog/sima-generalist-ai-agent-for-3d-virtual-environments/.
- Hugo Touvron, Thibaut Lavril, Gautier Izacard, Xavier Martinet, Marie-Anne Lachaux, Timothée Lacroix, Baptiste Rozière, Naman Goyal, Eric Hambro, Faisal Azhar, Aurelien Rodriguez, Armand Joulin, Edouard Grave, and Guillaume Lample. Llama: Open and efficient foundation language models. *arxiv preprint arXiv:2302.13971*, 2023a. URL https://arxiv.org/abs/2302.13971.
- Hugo Touvron, Louis Martin, Kevin Stone, Peter Albert, Amjad Almahairi, Yasmine Babaei, Nikolay Bashlykov, Soumya Batra, Prajjwal Bhargava, Shruti Bhosale, Dan Bikel, Lukas Blecher, Cristian Canton Ferrer, Moya Chen, Guillem Cucurull, David Esiobu, Jude Fernandes, Jeremy Fu, Wenyin Fu, Brian Fuller, Cynthia Gao, Vedanuj Goswami, Naman Goyal, Anthony Hartshorn, Saghar Hosseini, Rui Hou, Hakan Inan, Marcin Kardas, Viktor Kerkez, Madian Khabsa, Isabel Kloumann, Artem Korenev, Punit Singh Koura, Marie-Anne Lachaux, Thibaut Lavril, Jenya Lee, Diana Liskovich, Yinghai Lu, Yuning Mao, Xavier Martinet, Todor Mihaylov, Pushkar Mishra, Igor Molybog, Yixin Nie, Andrew Poulton, Jeremy Reizenstein, Rashi Rungta, Kalyan Saladi, Alan Schelten, Ruan Silva, Eric Michael Smith, Ranjan Subramanian, Xiaoqing Ellen Tan, Binh Tang, Ross Taylor, Adina Williams, Jian Xiang Kuan, Puxin Xu, Zheng Yan, Iliyan Zarov, Yuchen Zhang, Angela Fan, Melanie Kambadur, Sharan Narang, Aurelien Rodriguez, Robert Stojnic, Sergey Edunov, and Thomas Scialom. Llama 2: Open foundation and fine-tuned chat models. *arxiv preprint arXiv:2307.09288*, 2023b. URL https://arxiv.org/abs/2307.09288.
- Michael Tschannen, Cian Eastwood, and Fabian Mentzer. Givt: Generative infinite-vocabulary transformers. In *Proc. European Conference on Computer Vision (ECCV)*, pp. 292–309, Cham, 2025a. Springer Nature Switzerland.

- Michael Tschannen, André Susano Pinto, and Alexander Kolesnikov. Jetformer: An autoregressive generative model of raw images and text. In *Proc. International Conference on Learning Representation (ICLR)*, 2025b.
- Arnon Turetzky, Nimrod Shabtay, Slava Shechtman, Hagai Aronowitz, David Haws, Ron Hoory, and Avihu Dekel. Continuous speech synthesis using per-token latent diffusion. *arXiv* preprint *arXiv*:2410.16048, 2024. URL https://arxiv.org/abs/2410.16048.
- Aaron van den Oord, Oriol Vinyals, and Koray Kavukcuoglu. Neural discrete representation learning. In *Proc. Advances in Neural Information Processing Systems (NeurIPS)*, 2017.
- Ashish Vaswani, Noam Shazeer, Niki Parmar, Jakob Uszkoreit, Llion Jones, Aidan N Gomez, Ł ukasz Kaiser, and Illia Polosukhin. Attention is all you need. In *Proc. Advances in Neural Information Processing Systems (NeurIPS)*, 2017.
- Ilpo Viertola, Vladimir Iashin, and Esa Rahtu. Temporally aligned audio for video with autoregression. In *Proc. IEEE Int. Conf. Acoust., Speech, Signal Process. (ICASSP)*. IEEE, 2025.
- Pascal Vincent. A connection between score matching and denoising autoencoders. *Neural Computation*, 23(7):1661–1674, 2011.
- Heng Wang, Jianbo Ma, Santiago Pascual, Richard Cartwright, and Weidong Cai. V2a-mapper: A lightweight solution for vision-to-audio generation by connecting foundation models. In *Proc. AAAI Conference on Artificial Intelligence (AAAI)*, 2024a.
- Yongqi Wang, Wenxiang Guo, Rongjie Huang, Jiawei Huang, Zehan Wang, Fuming You, Ruiqi Li, and Zhou Zhao. Frieren: Efficient video-to-audio generation network with rectified flow matching. In *Proc. Advances in Neural Information Processing Systems (NeurIPS)*, volume 37, 2024b.
- Yusong Wu\*, Ke Chen\*, Tianyu Zhang\*, Yuchen Hui\*, Taylor Berg-Kirkpatrick, and Shlomo Dubnov. Large-scale contrastive language-audio pretraining with feature fusion and keyword-to-caption augmentation. In *Proc. IEEE Int. Conf. Acoust., Speech, Signal Process. (ICASSP)*, 2023.
- Yazhou Xing, Yingqing He, Zeyue Tian, Xintao Wang, and Qifeng Chen. Seeing and hearing: Open-domain visual-audio generation with diffusion latent aligners. In *Proc. IEEE Conference on Computer Vision and Pattern Recognition (CVPR)*, 2024.
- Biao Zhang and Rico Sennrich. Root mean square layer normalization. In H. Wallach, H. Larochelle, A. Beygelzimer, F. d'Alché-Buc, E. Fox, and R. Garnett (eds.), *Proc. Advances in Neural Information Processing Systems (NeurIPS)*, volume 32. Curran Associates, Inc., 2019. URL https://proceedings.neurips.cc/paper\_files/paper/2019/file/1e8a19426224ca89e83cef47f1e7f53b-Paper.pdf.
- Lvmin Zhang, Anyi Rao, and Maneesh Agrawala. Adding conditional control to text-to-image diffusion models. In *Proc. IEEE International Conference on Computer Vision (ICCV)*, pp. 3836–3847, October 2023.
- Yiming Zhang, Yicheng Gu, Yanhong Zeng, Zhening Xing, Yuancheng Wang, Zhizheng Wu, and Kai Chen. Foleycrafter: Bring silent videos to life with lifelike and synchronized sounds. *arXiv* preprint arXiv:2407.01494, 2024. URL https://arxiv.org/abs/2407.01494.
- Zhi Zhong, Akira Takahashi, Shuyang Cui, Keisuke Toyama, Shusuke Takahashi, and Yuki Mitsufuji. Specmaskfoley: Steering pretrained spectral masked generative transformer toward synchronized video-to-audio synthesis via controlnet. In *Proc. IEEE Int. Workshop Appl. Signal Process. Audio Acoust. (WASPAA)*, 2025.
- Linqi Zhou, Stefano Ermon, and Jiaming Song. Inductive moment matching. In *Proc. International Conference on Machine Learning (ICML)*, 2025. URL https://openreview.net/forum?id=pwNSUo7yUb.

#### **CONTENTS** Introduction **Preliminaries** 2.3 **SoundReactor** Problem Setup: Frame-level Online Video-to-Audio Generation . . . . . . . . . . . 3.2 3.3 3.4 **Experiments** 4.1 4.2 4.3 4.5 Conclusion Related Work **Experimental Details** B.2 B.3 B.4 B.6 C Additional Experiments

### A RELATED WORK

1080

1082

1083 1084

1086 1087

1088

1089

1090

1091

1092

1093

1094

1095

1096

1099

1100

1101 1102 1103

1104

1105

1106

1107

1108

1109

1110

1111

1113

1114

1115

1116

1117

1118

1119

1120

1121

1122

1123

1124

1125 1126

1127 1128

1129

1130 1131

1132

1133

### A.1 VIDEO-TO-AUDIO GENERATION

Offline video-to-audio (V2A) generation has been explored using both autoregressive (AR) and non-autoregressive (Non-AR) models.

**AR models.** AR models for V2A have focused on generating discrete audio tokens. One line of work operates on VQ-VAE (van den Oord et al., 2017) latents derived from Mel-spectrograms, which requires a separate vocoder for waveform synthesis. This category includes SpecVQGAN (Iashin & Rahtu, 2021), which uses a transformer to generate code indices from video RGB and optical flow; Im2Wav (Sheffer & Adi, 2023), which adopts a dual-transformer architecture conditioned on CLIP (Radford et al., 2021) features; and CondFoleyGen (Du et al., 2023), which uses ResNet (2+1)D-18 vision encoder (He et al., 2016). Another line of AR models utilizes discrete tokenizers based on raw waveforms using RVQ (Défossez et al., 2023; Kumar et al., 2023). In this paradigm, FoleyGen (Mei et al., 2024b) explores various vision encoders like CLIP and ImageBind (Girdhar et al., 2023), while V-AURA (Viertola et al., 2025) has achieved state-of-the-art performance in this category by introducing Synchformer (Iashin et al., 2024) video encoder, which enabled semantic and strong temporal alignment. The Synchformer's video encoder, a Motionformer (Patrick et al., 2021; Bertasius et al., 2021) relies on non-causal attention over video chunks. While suitable for the offline task, this makes V-AURA incompatible with our scope, the frame-level online V2A task. Our framework, SoundReactor, is categorized in this AR paradigm based on continuous audio latents and is applicable for both the offline and frame-level online V2A tasks.

**Non-AR models.** Non-AR models have also been widely investigated. The first direction involves training models from scratch based on Diffusion Models (DMs) (Ho et al., 2020) and Flow-matching Models (FMs) (Liu et al., 2023b). For instance, Diff-Foley (Luo et al., 2023) uses a CAVP (Luo et al., 2023) vision encoder to train DMs on Mel-spectrogram latents, while MultiFoley (Chen et al., 2025) applies a similar approach to latents derived from raw waveforms projected by DAC-based VAE (Kumar et al., 2023). Models such as Frieren (Wang et al., 2024b) and MMAudio (Cheng et al., 2025) leverage FMs; Frieren uses CAVP, whereas MMAudio employs a multimodal diffusion transformer (Esser et al., 2024) with CLIP and Synchformer encoders. ThinkSound (Liu et al., 2025) builds upon a multimodal LLM framework that uses Chain-of-Thought reasoning, followed by the MMAudio-style audio generator. A second direction is training models from scratch based on discrete tokens using MaskGIT (Chang et al., 2022). VATT (Liu et al., 2024a) employs a twostage pipeline where it first generates a text caption from the video and then uses MaskGIT to predict code indices of EnCodec (Défossez et al., 2023). MaskVAT (Pascual et al., 2024) applies MaskGIT to predict code indices of DAC conditioned on CLIP and SparseSync (Iashin et al., 2022) features. The third major trend is an adaptation of pre-trained text-to-audio models. Several methods steer AudioLDM (Liu et al., 2023a); ReWaS (Jeong et al., 2024) uses a ControlNet-based approach (Zhang et al., 2023) with an energy curve from the Synchformer; V2A-Mapper (Wang et al., 2024a) employs a lightweight network to map CLIP embeddings to CLAP embeddings (Wu\* et al., 2023); Seeing & Hearing (Xing et al., 2024) conditions the generator using ImageBind as a multimodal aligner; and FoleyCrafter (Zhang et al., 2024) fine-tunes it using an adapter-based method with CLIP features and a learnable timestamp adapter. Other backbones are also adapted, such as SpecMaskGIT (Comunità et al., 2024) by SpecMaskFoley (Zhong et al., 2025) and Stable Audio Open (Evans et al., 2025) by CAFA (Benita et al., 2025), both using ControlNet with CLIP and Synchformer features.

# A.2 AR AUDIO GENERATION WITHOUT VECTOR QUANTIZATION

Our work builds upon the emerging paradigm of AR audio generation with continuous audio latents. Prior work in this area has focused on unimodal audio domains such as unconditional music generation (CAM (Pasini et al., 2024)) and speech synthesis (DiTAR (Jia et al., 2025), SALAD (Turetzky et al., 2024), MELLE (Meng et al., 2025)). Concurrently, CALM (Rouard et al., 2025) adopts a MAR-style framework (Li et al., 2024) for speech and music continuation, using a consistency model-based head. Our work is distinct from this prior and concurrent work in two key aspects. First, to our best knowledge, we are the first to tackle an audio-visual multimodal task within this paradigm, where

# Algorithm 1 SoundReactor-Diffusion's training

```
1135
                      Require: Dataset \mathcal{D}
1136
                        1: repeat
                                       Sample (\{\mathbf{x}_1^0, \dots, \mathbf{x}_n^0\}, \{\mathbf{v}_1, \dots, \mathbf{v}_n\}) \sim \mathcal{D}, \epsilon_i \sim \mathcal{N}(0, I), t \sim p(t) \{\mathbf{v}_1, \dots, \mathbf{v}_n\} \leftarrow \varnothing \text{ with } p_{\text{uncond}} \mathbf{x}_i^t \leftarrow \mathbf{x}_i^0 + t \, \epsilon_i
1137
                                                                                                                                                                                                                        \triangleright \ln t \sim \mathcal{N}(P_{\text{mean}}, P_{\text{std}})
                        2:
                                                                                                                                                                                                                              ▷ Ø: null-embedding
1138
                        3:
                        4:
1139
                                        \mathbf{z}_i \leftarrow F_{\boldsymbol{\phi}}(\mathbf{v}_{\leq i}, \mathbf{x}_{< i}^0)
                        5:
1140
                                        \mathcal{L}_{\text{Stage1}}(\boldsymbol{\theta}, \boldsymbol{\phi}) \leftarrow \lambda(t)e^{-u_{\boldsymbol{\theta}}(t)} \sum_{i=1}^{n} \left\| \mathbf{x}_{i}^{0} - D_{\boldsymbol{\theta}}(\mathbf{x}_{i}^{t}, t, \mathbf{z}_{i}) \right\|_{2}^{2} + u_{\boldsymbol{\theta}}(t)
1141
1142
                                        Update (\boldsymbol{\theta}, \boldsymbol{\phi}) \leftarrow (\boldsymbol{\theta}, \boldsymbol{\phi}) - \eta \nabla_{(\boldsymbol{\theta}, \boldsymbol{\phi})} \mathcal{L}_{\text{Stage1}}
1143
                        8: until converged
1144
                        9: return (\boldsymbol{\theta}, \boldsymbol{\phi})
1145
1146
                      Algorithm 2 SoundReactor-ECT's training
1147
1148
                      Require: Dataset \mathcal{D}, pretrained parameters (\tilde{\boldsymbol{\theta}}, \tilde{\boldsymbol{\phi}}), mapping m(r \mid t, \text{Iters}), weighting function w(t), metric
1149
                                function d,
                         1: Init: (\boldsymbol{\theta}, \boldsymbol{\phi}) \leftarrow (\tilde{\boldsymbol{\theta}}, \tilde{\boldsymbol{\phi}}), Iters \leftarrow 0
1150
                        2: repeat
1151
```

```
Sample (\{\mathbf{x}_1^0,\ldots,\mathbf{x}_n^0\},\{\mathbf{v}_1,\ldots,\mathbf{v}_n\}) \sim \mathcal{D}
1152
                                                             Sample \epsilon_i \sim \mathcal{N}(0, I), t \sim p(t), r \sim m(r \mid t, \text{Iters})
                                                                                                                                                                                                                                                                                                                                            \triangleright \ln t \sim \mathcal{N}(P_{\text{mean}}, P_{\text{std}})
                                                         Sample \epsilon_i \sim \mathcal{N}(0, 1), t \sim P(0), 1

\{\mathbf{v}_1, \dots, \mathbf{v}_n\} \leftarrow \varnothing \text{ with } p_{\text{uncond}}

\mathbf{x}_i^t \leftarrow \mathbf{x}_i^0 + t \, \boldsymbol{\epsilon}_i, \quad \mathbf{x}_i^r \leftarrow \mathbf{x}_i^0 + r \, \boldsymbol{\epsilon}_i, \quad \Delta t \leftarrow t - r

\mathcal{L}_{\text{Stage2}}(\boldsymbol{\theta}, \boldsymbol{\phi}) \leftarrow w(t) \sum_{i=1}^{r} d(G_{(\boldsymbol{\theta}, \boldsymbol{\phi})}(\mathbf{x}_i^t), G_{\text{sg}(\boldsymbol{\theta}, \boldsymbol{\phi})}(\mathbf{x}_i^r))
1153
                                     5:
                                                                                                                                                                                                                                                                                                                                                     ⊳ Ø: null-embedding
1154
                                    6:
1155
                                                                                                                                                                                                                                                                                                                                                                ▷ sg: stop-gradient
1156
1157
```

 $(oldsymbol{ heta}, oldsymbol{\phi}) \leftarrow (oldsymbol{ heta}, oldsymbol{\phi}) - \eta \, 
abla_{(oldsymbol{ heta}, oldsymbol{\phi})} \mathcal{L}_{ ext{Stage2}}(oldsymbol{ heta}, oldsymbol{\phi})$ 8: 9:  $sg(\boldsymbol{\theta}, \boldsymbol{\phi}) \leftarrow stopgrad(\mu sg(\boldsymbol{\theta}, \boldsymbol{\phi}) + (1 - \mu)(\boldsymbol{\theta}, \boldsymbol{\phi}))$  $\triangleright \mu$ : EMA rate

10: Iters  $\leftarrow$  Iters + 1

11: **until**  $\Delta t \rightarrow 0$ 

1134

1158

1159

1160

1161 1162 1163

1164

1165

1166

1167 1168

1169 1170

1171 1172

1173

1174

1175

1176

1177

1178

1179

1180

1181

1182

1183

1184

1185

1186

1187

12: return  $(\theta, \phi)$ 

we introduce and solve the novel task of frame-level online V2A generation (see Section 1 and 3.1 for comparison to the offline setup.). Second, regarding diffusion head acceleration, our work is complementary to CALM: we investigate the ECT framework (Geng et al., 2025b), in contrast to their sCM-based from-scratch training (Lu & Song, 2025).

#### В EXPERIMENTAL DETAILS

#### IMPLEMENTATION DETAILS B.1

**Vision token modeling** We adopt a pretrained DINOv2 vision encoder to extract grid features per video frame. We use grid features instead of the encoder's [CLS]-token because it lacks the temporal cues necessary for audio-visual synchronization. Our preliminary analysis, shown in Figure 5, reveals that the cosine similarities between (A) adjacent video frames (30FPS) and (B) every other frame (15FPS) are significantly high. We extract grid features from the final layer before the [CLS]-token head. We employ the dinov2-vits14-reg<sup>9</sup> (21 M parameters) for better per-frame encoding efficiency than larger backbones. Since raw grid features might be computationally expensive depending on a budget (e.g., training throughput and data storage), we first apply bilinear interpolation to halve both spatial dimensions. Second, we apply Principal Component Analysis (PCA) (Jolliffe, 2011) to reduce the hidden dimension from the original 384. We use 59, which preserves 70% of the cumulative explained variance (CEV) by default. These compressed features are precomputed before training. The adjacent frame subtraction is conducted on the precomputed grid features before being fed to the downstream projection layer described in Section 3.2 and Figure 2 (a). We use a 512-dimensional learnable aggregate token for the transformer aggregator. For the transformer

<sup>&</sup>lt;sup>8</sup>The average cosine similarity over 3, 830 video clips in our test split is  $0.99 \pm 0.0072$  for adjacent frames and  $0.98 \pm 0.010$  for every other frame.

https://github.com/facebookresearch/dinov2

1189

1211 1212

1213

1214 1215

1216

1217

1218

1219

1220 1221

1222

1223

1224

1225

1226

1227

1228 1229

1230 1231

1232

1233

1234

1236

1237

1239

1240

1241

# Algorithm 3 SoundReactor's frame-level online V2A sampling

```
Require: Video frames \{V_i\}_{i=1}^n (Raw videos); vision encoding module \mathcal{E}; transformer F_{\phi}; diffusion
1190
                        head D_{\theta}; waveform decoder \mathrm{Dec}_{\mathsf{VAE}}; null embedding \varnothing; guidance scale \omega; head mode mode \in
1191
                        {Diffusion, ECT}
1192
                  1: \mathbf{x}_0 \leftarrow \langle \text{BOS} \rangle
1193
                  2: for i = 1 ... n do
1194
                               \tilde{\mathbf{z}}_{2i-1} \leftarrow F_{\boldsymbol{\phi}}(\mathbf{x}_{i-1})
                               \begin{split} & \tilde{\mathbf{v}}_i \leftarrow \mathcal{E}(V_i) \\ & \tilde{\mathbf{z}}_{2i}^{\text{cond}}, \tilde{\mathbf{z}}_{2i}^{\text{null}} \right] \leftarrow F_{\boldsymbol{\phi}}([\mathbf{v}_i, \varnothing]) \\ & \tilde{\mathbf{z}}_{2i} \leftarrow \tilde{\mathbf{z}}_{2i}^{\text{null}} + \omega(\tilde{\mathbf{z}}_{2i}^{\text{cond}} - \tilde{\mathbf{z}}_{2i}^{\text{null}}) \end{split}
1195
                  4:
1196
                  5:
                                                                                                                                                  ▶ Batch process for CFG paths
1197
                  6:
                               \mathbf{z}_i \leftarrow \operatorname{Concat}(\tilde{\mathbf{z}}_{2i-1}, \, \tilde{\mathbf{z}}_{2i})
1198
                  7:
1199
                  8:
                               if mode = Diffusion then
                  9:
                                       \mathbf{x}_i \leftarrow \text{DiffusionSampling}(D_{\boldsymbol{\theta}}, \mathbf{z}_i)
                                                                                                                                                                   10:
                               else
1201
                                      \mathbf{x}_i \leftarrow \texttt{CMSampling}(D_{\boldsymbol{\theta}}, \mathbf{z}_i)
                                                                                                                                             \triangleright Few-step sampling (NFE=1\sim4)
                11:
1202
                12:
                               end if
1203
                               if streaming_decode and DecvaE is causal then
                13:
                14:
                                      \hat{\mathbf{y}}_{1:i} \leftarrow \mathrm{Dec}_{\mathrm{VAE}}(\{\mathbf{x}_j\}_{j=1}^i)
                                                                                                                                                                1205
                15:
                16: end for
1207
                17: if not streaming decode then
1208
                               \hat{\mathbf{y}}_{1:n} \leftarrow \mathrm{Dec}_{\mathrm{VAE}}(\{\mathbf{x}_i\}_{i=1}^n)
                                                                                                                                                         ▷ Decode all tokens at once
1209
                19: end if
1210
                20: return Waveform \hat{\mathbf{y}}_{1:n}
```

aggregator, we use a single non-causal transformer layer with learnable positional embeddings. We conduct ablation studies on these vision conditions in Appendix C.3.

**Audio token modeling** We follow the stereo VAE from SA Series (Evans et al., 2025; 2024) as a model backbone. We change the temporal downsampling rate from 2048 to 1600 and train with 48 kHz stereo waveform by using OGameData250K and WavCaps (Mei et al., 2024a) dataset from scratch. We follow the original training configuration (Evans et al., 2025). The network parameter size is 157 M. In the latent space, we get 64 dimensions of 30-Hz continuous audio latents.

Multimodal transformer with diffusion head For the multimodal AR transformer, we use 18 layers, 1024 hidden dimensions, and 16 heads. The model backbone follows LLaMA-style design (Touvron et al., 2023a;b), applying pre-normalization using RMSNorm (Zhang & Sennrich, 2019), SwiGLU activation (Shazeer, 2020), and rotary positional embeddings (RoPE) (Su et al., 2024). For the diffusion head, we set 8 blocks and a width of 1280 channels. The architecture of the diffusion head largely follows the original architecture in MAR. The total parameter size is 320 M (250 M for the transformer and 70 M for the diffusion head). We ablate various numbers of parameters of the diffusion head in Appendix C.1.

### **B.2** Training Details

**Stage-1: Diffusion pretraining** After obtaining  $\mathbf{x}^0$  through the audio VAE,  $\mathbf{x}^0$  is standardized globally to zero mean and standard deviation  $\sigma_{\text{data}} = 0.5$  by following EDM2 (Karras et al., 2024). We utilize the EDM's skip connection  $c_{\text{skip}}(t)$ , output scale  $c_{\text{out}}(t)$ , input scale  $c_{\text{in}}(t)$ , and  $c_{\text{noise}}(t)$  for modeling  $D_{\theta}$  as:

$$D_{\theta}(\mathbf{x}_{i}^{t}, t, \mathbf{z}_{i}) = c_{\text{skip}}(t) \,\mathbf{x}_{i}^{t} + c_{\text{out}}(t) \,\text{NN}_{\theta} \left(c_{\text{in}}(t) \,\mathbf{x}_{i}^{t}, c_{\text{noise}}(t), \mathbf{z}_{i}\right), \tag{9a}$$

$$c_{\rm skip}(t) = \sigma_{\rm data}^2 / (t^2 + \sigma_{\rm data}^2), \tag{9b}$$

$$c_{\text{out}}(t) = (t \,\sigma_{\text{data}}) / \sqrt{t^2 + \sigma_{\text{data}}^2},\tag{9c}$$

$$c_{\rm in}(t) = 1/\sqrt{t^2 + \sigma_{\rm data}^2},\tag{9d}$$

$$c_{\text{noise}}(t) = \frac{1}{4} \ln t, \tag{9e}$$

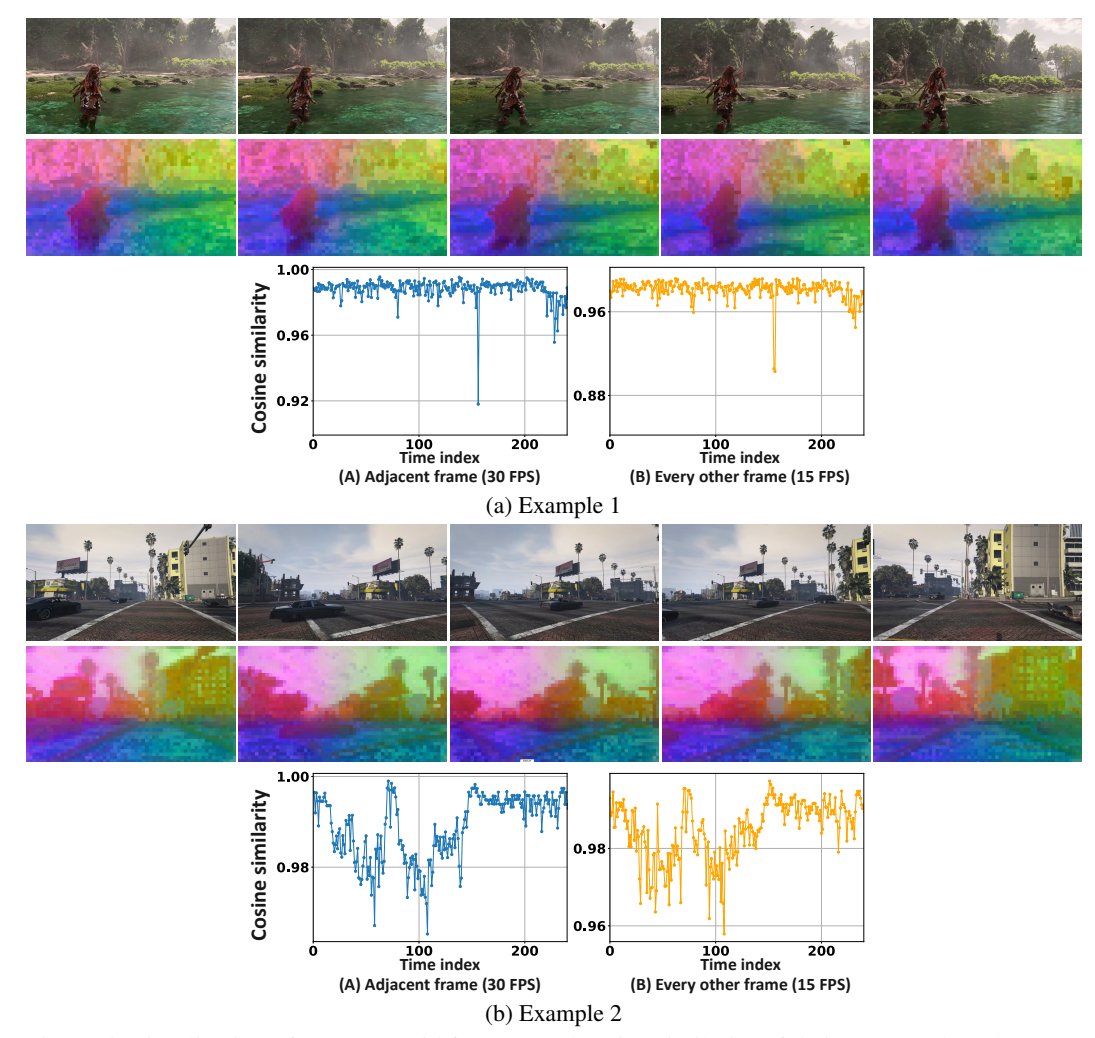


Figure 5: Visualization of DINOv2 grid features and cosine similarity of their [CLS]-tokens between (A) adjacent frames and (B) every other frame. Visualizations are done by applying PCA to grid features and mapping them to RGB.

where  $\mathrm{NN}_{\theta}$  is the actual neural network to be trained. We set  $P_{\mathrm{mean}} = -0.4$ ,  $P_{\mathrm{std}} = 1.0$  for a training noise sampling  $\ln t \sim \mathcal{N}(P_{\mathrm{mean}}, P_{\mathrm{std}})$  and network dropout rate of 10% (Srivastava et al., 2014). The models are trained using the AdamW optimizer (Loshchilov & Hutter, 2019) for 300K training iterations. Training is done on  $8\times\mathrm{NVIDIA}$  H100 GPUs. Training duration is around 36 hrs. Training is done with bf16. The weight decay and momenta for AdamW are 0.02 and (0.9, 0.95). We set a learning rate of 1e-4 with the constant learning rate scheduler, EMA rate of 0.9999, and gradient clipping as 1.0. By default, we use a batch size of 128. To enable CFG sampling on the transformer, during training, we randomly replace all the video tokens  $\mathbf{v}_i(i=1,\ldots,n)$  with the learnable null embedding with the probability of 10%. As our denoising network is not so large, we can sample t multiple times for any given  $\mathbf{z}_i$ . We sample t by 4 times during training for each sample by following (Li et al., 2024). This operation helps improve the utilization of the loss function.

**Stage-2: ECT** As same as Stage 1 network configuration, we utilize the EDM's skip connection  $c_{\text{skip}}(t)$ , output scale  $c_{\text{out}}(t)$ , input scale  $c_{\text{in}}(t)$ , and  $c_{\text{noise}}(t)$  for modeling the head. For a metric function d, we use a Pseudo-Huber loss  $d(\mathbf{a}, \mathbf{b}) = \sqrt{\|\mathbf{a} - \mathbf{b}\|_2^2 + \nu^2} - \nu$ , where  $\nu = 0.06$  (Song & Dhariwal, 2024; Geng et al., 2025b). By following the original work, we set  $P_{\text{mean}} = -0.8$ ,  $P_{\text{std}} = 1.6$  for a training noise sampling  $\ln t \sim \mathcal{N}(P_{\text{mean}}, P_{\text{std}})$ , and  $w(t) = 1/t^2 + 1/\sigma_{\text{data}}^2$ . For the mapping function  $m(r \mid t, \text{Iters})$  (in Eq 8), we explore two different setups suggested by the literature (Geng et al., 2025b), which we describe in Section 4.5. For CF (our default), we set q = 2,  $s = \text{total\_iter}//8$ , b = 1, k = 8 in Eq (8). For IN, we set q = 4,  $s = \text{total\_iter}//4$ , b = 1,

k=8. The models are trained using the AdamW optimizer (Loshchilov & Hutter, 2019) for 200K training iterations. Training is done on  $8\times NVIDIA$  H100 GPUs. Training duration is around 20 hours. Training is done with bf16. The weight decay and momenta for AdamW are 0.02 and (0.9, 0.95). We set a learning rate of 1e-4 with the constant learning rate scheduler, EMA rate of 0.9999 for  $sg(\theta,\phi)$ , batch size of 128, and gradient clipping as 1.0. To enable CFG sampling, we randomly replace the learnable null embedding with all the video tokens  $v_i(i=1,\ldots,n)$  with the probability of 10%. We sample t by 4 times during training for each sample by following the Stage 1 training.

### **B.3** Sampling Details

**AR transformer** Our sampling procedure follows that of a standard decoder-only AR transformer with a token-wise KV cache (Shazeer, 2019). As described in Section 3.4, to get  $\tilde{\mathbf{z}}_{2i}$  (a corresponding input token is a vision condition  $\mathbf{v}_i$ ), we apply CFG as  $\tilde{\mathbf{z}}_{2i} = \tilde{\mathbf{z}}_{2i}^{\text{null}} + \omega(\tilde{\mathbf{z}}_{2i}^{\text{cond}} - \tilde{\mathbf{z}}_{2i}^{\text{null}})$ , where  $\omega$  is a guidance scale,  $\tilde{\mathbf{z}}_{2i}^{\text{cond}}$  is the transformer output given the visual condition  $\mathbf{v}_i$ , and  $\tilde{\mathbf{z}}_{2i}^{\text{null}}$  is the output given a learnable null embedding, respectively. To get  $\tilde{\mathbf{z}}_{2i}^{\text{null}}$ , all the  $\mathbf{v}_{\leq i}$  are replaced with the learnable null embedding. Sampling is done with bf16.

Our approach contrasts with the CFG strategy in the original MAR (Li et al., 2024), where CFG is applied within the diffusion head. In the original MAR, the transformer generates both conditional  $\mathbf{z}_i^{\text{cond}}$  and unconditional  $\mathbf{z}_i^{\text{uncond}}$  vectors, which are then used for the standard CFG diffusion sampling. In contrast, we do not apply CFG within the diffusion head. We compare the performance of both CFG strategies in Appendix C.1. Our design choice has a practical benefit, except for the performance: it reduces the computational overhead during sampling on the diffusion head, which might be critical when the head becomes larger or using the head without sampling acceleration.

**Diffusion head** For the diffusion sampling on our Stage-1 model, we use the deterministic Heun solver with the same time-step discretizations as EDM (Karras et al., 2022; 2024). Namely, if we generate samples with N-steps,  $t_j = (t_{\max}^{1/\rho} + \frac{j}{N-1}(t_{\min}^{1/\rho} - t_{\max}^{1/\rho}))^{\rho}$ , where  $\rho = 7$ . On our Stage-2 model, we set intermediate time step t = 2.5 and t = [5.0, 1.1, 0.08] on NFE=2 and NFE=4, respectively. We use the EMA weights during sampling and set  $\{t_{\max}, t_{\min}\} = \{80, 0.00\}$  on the both Stage-1 and Stage-2 (Karras et al., 2022; 2024; Song & Dhariwal, 2024; Geng et al., 2025b). Sampling is done with bf16. We provide the sampling procedure in Algorithm 3.

### B.4 CONTEXT WINDOW EXTENSION ON ROPE

In Section 4.4, we test our model on longer sequence generation beyond the training context window up to twice the training window on SoundReactor-ECT with NFE=4. In the experiments, we examine two zero-shot context window extension methods based on RoPE, Position Interpolation (PI) (Chen et al., 2023) and NTK-aware interpolation (NTK) (Tancik et al., 2020), and Sliding Window Attention (SWA) (Beltagy et al., 2020; Jiang et al., 2023). Here, we describe those methods.

RoPE is applied to both the query (q) and key (k) vectors within a transformer layer. An input token  $\mathbf{z}_i$  is first projected into a query vector  $\mathbf{q}_i = W_q \mathbf{z}_i$  and a key vector  $\mathbf{k}_i = W_k \mathbf{z}_i$ , where  $\mathbf{q}_i, \mathbf{k}_i \in \mathbb{R}^{c_z}$ . To encode the positional information, the  $\mathbf{q}_i$  is treated as a sequence of two-dimensional vectors  $(q_{i,2l-1},q_{i,2l})$ , where l is the index ranging from 1 to  $c_{\mathbf{z}}/2$ . A rotation is then applied to each pair as follows:

$$\begin{pmatrix} q'_{i,2l-1} \\ q'_{i,2l} \end{pmatrix} = \begin{pmatrix} \cos i\varphi_l & -\sin i\varphi_l \\ \sin i\varphi_l & \cos i\varphi_l \end{pmatrix} \begin{pmatrix} q_{i,2l-1} \\ q_{i,2l} \end{pmatrix}, \tag{10}$$

where the frequency  $\varphi_l = \xi^{-2l/c_z}$  depends on the index l and a base  $\xi$ . The same process is applied to the key vector  $\mathbf{k}_i$ .

**Position interpolation (PI)** PI adapts RoPE to longer sequences by down-scaling the position indices via  $i' = i \cdot (n/n')$ , where n and n' are a training sequence length and a target sequence length during inference, respectively. This operation uniformly compresses the entire frequency spectrum, which can degrade the model's understanding of high-frequency details essential for precise temporal alignment.

**NTK-aware interpolation (NTK)** Instead of scaling the position indices, NTK scales the base  $\xi$  of the frequency calculation to a new value  $\xi' = \xi \cdot (n'/n)^{c_{\mathbf{z}}/(c_{\mathbf{z}}-2)}$ . The approach is motivated by Neural Tangent Kernel theory (Tancik et al., 2020), which posits that deep neural networks have trouble learning high-frequency information if the input dimension is low without the corresponding embeddings having high-frequency components. NTK's base rescaling allows the model to retain its modeling capabilities on high-frequency information, which we qualitatively observe in Figure 3.

**Sliding window attention (SWA)** Besides extending the context window, SWA is one of the standard and efficient attention mechanisms that restricts each token to only attend to a fixed-size local window of preceding tokens. For generation beyond the training context window, it simply continues to apply this local attention window. While this approach is computationally efficient, its ability to model long-range dependencies is inherently limited by the fixed window size.

**Discussion** In addition to quantitative evaluation in Section 4.4, the spectrogram visualization in Figure 3 shows that PI slows periodic sounds (e.g., footsteps) and harms temporal synchronization, while NTK and SWA preserve timing. We conjecture that this stems from how RoPE frequencies are scaled. Our interleaved, frame-aligned audio–visual tokens rely on high-frequency positional components for the precise timing of action sounds. NTK rescales the RoPE base and preserves high-frequency structure via  $\xi' = \xi \cdot (n'/n)^{c_z/(c_z-2)}$ . In contrast, PI stretches positions in the time domain  $i' = i \cdot (n/n')$ , which lowers the angular frequency. This experiment is complementary to prior findings from the other domains, such as language domain, by demonstrating the superiority of NTK over PI in a multimodal audio-visual setting. We validate its effectiveness through not only the quantitative performance difference but also the qualitative analysis of the spectrograms.

### B.5 Per-frame Latency Measurement

We measure two metrics: wave-level and token-level latency. Wave-level latency is the elapsed time from feeding the previous audio token  $\mathbf{x}_{n-1}$  into the model until the output  $\mathbf{x}_n$  is incrementally decoded into a waveform, including the encoding of the raw video frame  $V_n$ . Token-level latency is identical to this but excludes the incremental waveform decoding. Following Algorithm 3, we insert torch.cuda.synchronize() calls between lines 2–3 and 14–15 to measure wave-level latency, and between lines 2–3 and 11–12 to measure token-level latency. This duration is recorded as the per-frame latency. For each video, we average the per-frame latencies over all frames except the initial one. We perform this benchmark on a single H100 GPU with a batch size of one, using a single CUDA stream for the entire pipeline. We use 53 clips (30FPS, 480p, 16 second) with the default SoundReactor-ECT at  $\omega=3$ . We use NTK to generate 16 seconds with KV-cache<sup>10</sup>. We apply FlashAttention-2 (Dao, 2024) for the main model. The torch.compile is enabled on the main model while CUDA Graph is used on the VAE decoder. To measure the wave-level latency, we use a causal stereo full-band VAE, which is created by fine-tuning our default VAE to make the decoder causal while freezing the encoder parameters.

We provide the mean and standard deviation over the 50 clips following a 3-clip warm-up period  $^{11}$ . As demonstrated in Table 6, while our model achieves remarkably low per-frame token-level latency, the overhead from incremental waveform decoding prevents the end-to-end wave-level latency from meeting the 33.3 ms threshold (per-frame real-time for 30FPS video). In terms of sample quality, we observe that the causal VAE decoder lags behind its non-causal counterpart in reconstruction quality (causal:  $rMMD_{OpenL3} = 62.7$ ,  $rMMD_{CLAP} = 0.538$ ; non-causal:  $rMMD_{OpenL3} = 60.4$ ,  $rMMD_{CLAP} = 0.301$ ). This performance gap propagates to final generation quality: e.g., our model on ECT (NFE=4) with the causal decoder yields  $MMD_{OpenL3} = 65.5$  and  $MMD_{CLAP} = 0.682$ , versus 64.6 and 0.451 with the non-causal one (our default setup). Accordingly, addressing the causal VAE's decoding overhead and fidelity gap remains an important direction for our future work.

# B.6 METRICS DETAILS

**Audio quality** To evaluate audio quality, we use Frechet Audio Distance (FAD) (Gui et al., 2024), Maximum Mean Discrepancy (MMD) (Chung et al., 2025; Jayasumana et al., 2024), and

<sup>&</sup>lt;sup>10</sup>NTK, PI, and no RoPE extension do not affect latency.

<sup>&</sup>lt;sup>11</sup>This is for excluding system warm-up effects, such as GPU kernel initialization.

Kullback-Leibler divergence based on PaSST (Koutini et al., 2022) (KL<sub>PaSST</sub>). For FAD and MMD, following prior work Evans et al. (2024; 2025); Gui et al. (2024), we use OpenL3 (Cramer et al., 2019) and LAION-CLAP (Wu\* et al., 2023). For OpenL3, we use (Env, Mel256, 512) in https://github.com/torchopenl3/torchopenl3. For CLAP, we use the 630k-audioset-fusion-best.pt from https://github.com/LAION-AI/CLAP as audio feature extractors. Since our model is trained on stereo signals, we compute the metrics on four channel configurations: the left channel (Left), the right channel (Right), their average (Center), and their difference (Diff) (Steinmetz et al., 2021). We compute KL<sub>PaSST</sub> only on the Center. For the samples from the models trained on monaural signal, they are duplicated for the left and right channels. Consequently, the Diff is omitted as the difference becomes zero. Furthermore, as a complementary metric to evaluate stereo quality, we also use Frechet Stereo Audio Distance (FSAD) (Sun et al., 2025), which is based on StereoCRW (Chen et al., 2022b) features.

**Audio-visual alignment** To evaluate audio-visual semantic and temporal alignment, we utilize ImageBind score (IB-Score) (Girdhar et al., 2023) and DeSync (Viertola et al., 2025) by following common practices (Cheng et al., 2025; Viertola et al., 2025). To compute DeSync, we take two crops (first 4.8 sec. and last 4.8 sec.) from the video and compute the average over the results (Cheng et al., 2025). We compute these two metrics only on the Center.

### C ADDITIONAL EXPERIMENTS

### C.1 ABLATION STUDY ON GENERATOR TRAINING

Diffusion head size In Table 7, we analyze the capacity of the diffusion head while keeping the total model parameters fixed at 320 M parameters. We use 35 (60%CEV) for this experiment. A larger head consistently yields better generation quality. Notably, while the original MAR generates valid images even with very small heads (e.g., 2M and 6M parameters).

Table 7: Ablation study on various sizes of diffusion head on SoundReactor-Diffusion under a fixed entire network capacity. Bold and underlined scores indicate the best and second-best results, respectively.

		MN	ſD↓					
Head size	OpenL3		CLAP		$KL_{PaSST} \downarrow$	IB-Score ↑	DeSync ↓	
	Center	Diff	Center	Diff				
10M	76.4	45.0	0.943	1.44	1.66	0.277	1.06	
30M	68.3	37.0	0.684	1.31	1.56	0.280	1.03	
50M	68.4	<u>35.5</u>	0.628	1.25	1.56	0.280	1.04	
70M (default)	69.3	35.1	0.597	1.29	1.56	0.280	1.03	

eters) (Li et al., 2024), our 10M head variant failed to produce high-quality samples. We hypothesize this is due to the challenge of handling high-dimensional audio tokens ( $c_{\rm x}=64$ )<sup>12</sup>. Indeed, our preliminary trials on an even higher dimension of  $c_{\rm x}=128$  yielded no valid audio even with a 50 M head. Consequently, the necessity of allocating substantial capacity to the diffusion head directly slows down decoding speed per token, providing a strong motivation for the step-wise acceleration that we introduce in this work.

**ECT strategy regarding fine-tuning component** We conduct an ablation study on two ECT fine-tuning strategies: fine-tuning only the diffusion head and fine-tuning the entire network (our default setup). As shown in Table 8, fine-tuning the entire network yields superior overall performance. However, we newly find that, interestingly, fine-tuning only the diffusion head is still

Table 8: ECT fine-tuning with the entire network (Our default) and only with the diffusion head (Only head). We use IN-0.2. MMD is computed on Center.

Model	MM	D↓	KL <sub>PaSST</sub> ↓	IB-Score ↑	DeSvnc ↓	
	OpenL3	CLAP			,	
Only head						
IN-0.2 (NFE=2)	68.7	0.623	1.59	0.272	1.05	
IN-0.2 (NFE=4)	62.1	0.585	1.61	0.272	1.03	
Our default						
IN-0.2 (NFE=2)	71.65	0.445	1.57	0.284	1.03	
IN-0.2 (NFE=4)	59.79	0.411	1.56	0.280	1.03	

sufficient to generate good audio samples. This insight suggests a potential path toward more efficient step-wise acceleration on the diffusion heads.

### C.2 ABLATION STUDY ON SAMPLING STRATEGY

Here, we analyze the model's behavior with various sampling strategies. Figure 6 shows the objective metrics for SoundReactor-Diffusion with various numbers of sampling steps, with the fixed guidance

<sup>&</sup>lt;sup>12</sup>A similar discussion has been reported in https://github.com/LTH14/mar/issues/55.

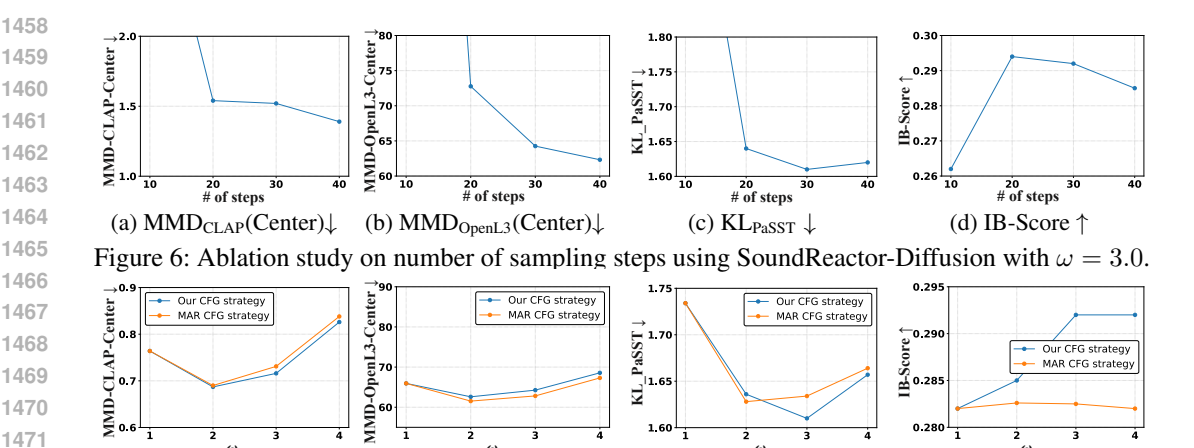


Figure 7: Ablation study on CFG scale  $\omega$  using SoundReactor-Diffusion with 30 steps. Differences between our strategy and MAR's are described in Appendix B.3.

(c)  $KL_{PaSST} \downarrow$ 

(d) IB-Score ↑

(b) MMD<sub>OpenL3</sub>(Center)↓

scale  $\omega=3.0$ . We observe that 10 steps (NFE=19) fail to generate valid samples, 20 steps (NFE=39) begin to yield reasonable samples, and 30 (NFE=59) or more steps are required for high-quality samples. These results motivate us to conduct diffusion head acceleration to achieve low per-frame latency.

In Figure 7, we fix the number of steps to 30 and examine the impact of the CFG scale  $\omega$ . The results indicate an optimal performance range between  $\omega=2.0$  and  $\omega=3.0$ . We also include results from applying the original MAR's CFG strategy to our models. Concretely,  $\mathbf{z}_i^{\text{cond}} = \text{Concat}(\tilde{\mathbf{z}}_{2i-1}, \tilde{\mathbf{z}}_{2i}^{\text{cond}})$  and  $\mathbf{z}_i^{\text{uncond}} = \text{Concat}(\tilde{\mathbf{z}}_{2i-1}, \tilde{\mathbf{z}}_{2i}^{\text{cull}})$  are used to conduct CFG sampling on the diffusion head (See the difference from our strategy explained in Algorithm 3 and Appendix B.3). While both strategies perform comparably, our approach is more computationally efficient, as noted in Appendix B.3, since our strategy does not use CFG on either diffusion or CM sampling.

Figure 8 presents the objective metrics for SoundReactor-ECT across various NFEs and  $\omega$  values. Similar to the results for SoundReactor-Diffusion, we observe a consistent performance sweet spot around  $\omega=2.0$  and  $\omega=3.0$  for all evaluated NFEs on the head.

### C.3 ABLATION STUDY ON VISION CONDITIONING

Influence of dimensionality reduction via PCA To investigate the influence of dimensionality reduction on the pretrained grid features by PCA (See Appendix B.1), we train the models with feature dimensions of 35, 59, and 99 dimensions, corresponding to CEV levels of 60%, 70%, and 80%, respectively. All models in this specific experiment are trained with half the default batch size. As shown in Ta-

(a) MMD<sub>CLAP</sub>(Center)↓

Table 9: Varying dimensionality of PCA-reduced features and the impact of using our adjacent frame subtraction. Tested on SoundReactor-Diffusion. Bold and underlined scores indicate the best and second-best results, respectively.

Channel-dim	MM	D↓	KL <sub>PaSST</sub> ↓	IB-Score ↑	DeSync ↓	
	OpenL3 CLAP		rassr y			
35 (60% CEV)	62.8	0.669	1.79	0.281	1.07	
w/o. subtraction	71.2	0.697	1.60	0.290	1.04	
59 (default) (70% CEV)	63.9	0.666	1.60	0.285	1.06	
w/o. subtraction	74.7	0.831	1.75	0.292	1.07	
99 (80% CEV)	67.4	0.655	1.59	0.284	1.04	
w/o. subtraction	72.1	0.715	1.61	0.293	1.05	

ble 9, interestingly, even the compressed representation achieves better results on several metrics compared to its higher-dimensional counterparts. Although the dimensionality necessary for modeling is expected to vary across data distributions, our empirical results suggest that vision conditioning might be feasible with compact representations derived from a selected subset of salient features.

**Effectiveness of adjacent frame subtraction** We ablate our vision conditioning mechanism that utilizes temporal differences between adjacent grid features (described in Section 3.2). As demonstrated in Table 9, removing this component consistently degraded performance. This indicates that incorporating temporal information via frame differencing is a crucial component of our vision conditioning.

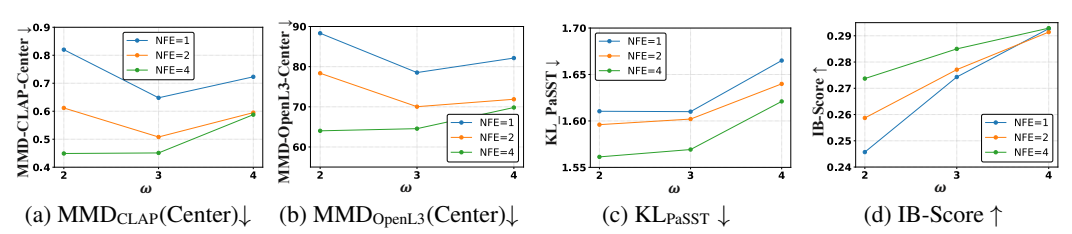


Figure 8: Ablation study on CFG scale  $\omega$  using SoundReactor-ECT with various NFEs on head.

### C.4 SUPPLEMENTARY EXPERIMENTS ON VGGSOUND

### C.4.1 EXPERIMENTAL SETUP

 As a supplementary evaluation, we benchmark our framework against various offline V2A approaches on the VGGSound dataset (Chen et al., 2020b). VGGSound consists of 200K+10-second (around 500 hours) real-world uncurated video clips from YouTube spanning 309 categories. We follow the data split and preprocessing pipeline in MMAudio (Cheng et al., 2025), where the training set contains approximately 180K 8-second videos (around 400 hours). We use only audio-visual pairs, without their corresponding class labels. All data is processed at 30 FPS with  $640 \times 360$  resolution and 48kHz stereo audio. For evaluation, consistent with previous work (Cheng et al., 2025; Zhong et al., 2025), we use 8-second clips from the VGGSound test set (15K videos).

For objective metrics, we use Frechet Audio Distance (FAD<sub>PaSST</sub>) (Gui et al., 2024) and Kullback–Leibler divergence (KL<sub>PaSST</sub>) based on PaSST (Koutini et al., 2022), a 32 kHz state-of-the-art audio classifier. For audio-visual alignment, we use ImageBind score (IB-Score) (Girdhar et al., 2023) and DeSync (Viertola et al., 2025), which is computed on the features extracted by Synchformer. We only compute these metrics on Center, derived by averaging the left and right channels.

For the model training, we largely follow the default setup from our OGameData experiments (detailed in Appendix B), with the following exceptions: we use a three-layer non-causal transformer for the aggregator (instead of a single layer), a 768-dimensional learnable token (instead of 512-dimensional), and reduce the DINOv2 (dinov2-vits14-reg) grid feature dimension to 146 via PCA, retaining the CEV of 80%. For inference, we set  $\omega=4.0$  across all experiments and use a 30-step deterministic Heun Solver for SoundReactor-Diffusion. For SoundReactor-ECT, we set intermediate time step t=2.5 and t=[5.0,1.1,0.08] on NFE=2 and NFE=4, respectively. We use the causal stereo full-band VAE, which is created by fine-tuning our default VAE to make both the encoder and decoder causal, for this experiment.

# C.4.2 RESULTS

The results are presented in Table 10, with details of the baseline methods in Appendix A.1. Compared to the offline AR model, V-AURA, our framework shows a similar trend on FAD<sub>PaSST</sub> and DeSync as in the OGameData experiments, though it lags behind on IB-Score and KL<sub>PaSST</sub>. Against offline Non-AR models, our framework outperforms several methods such as Seeing & Hearing, ReWaS, and FoleyCrafter, while a significant performance gap remains with MMAudio, which is the state-of-the-art V2A model<sup>13</sup>. Overall, these results demonstrate that our framework is generalizable to real-world video datasets, despite some performance limitations. Demo samples of the VGGSound are available at https://anonymous-sr-submission.github.io/vggsound.html.

Potential avenues for bridging this performance gap include using larger image encoders such as CLIP-L (300M) and CLIP-H (840M) that used in the baselines (or the larger variants of DINOv2) or employing video encoders pre-trained on large-scale audio-visual datasets, which can extract video features under a causal constraint. However, designing effective architectures that incorporate these components while preserving the end-to-end causality and low frame-level latency, which are crucial for the online V2A task, is a non-trivial challenge. Therefore, we leave this as future work.

<sup>&</sup>lt;sup>13</sup>We also observe that the DeSync appears to favor models that use Synchformer features, such as SpecMask-Foley, V-AURA, and MMAudio, which outperform the VAE reconstruction, suggesting a potential methodological bias

Table 10: Additional experiments on VGGSound test set with various offline V2A models. Only our models are applicable to frame-level online V2A task, which is our focus on this work. Following common practice (Cheng et al., 2025), parameter counts only on generative modeling part.

Model	Params	Channels/ Sample rate	Text condition	$FAD_{PaSST} \downarrow$	$KL_{PaSST} \downarrow$	IB-Score ↑	DeSync ↓
Our VAE-Reconstruction	=	2/48kHz	=	57.0	0.361	27.0	0.70
Offline AR models							
V-AURA (Viertola et al., 2025)	695M	1/44.1kHz	×	219	2.07	0.28	0.65
Offline Non-AR models							
Frieren (Wang et al., 2024b)	159M	1/16kHz	×	106	2.86	0.23	0.85
V2A-Mapper (Wang et al., 2024a)	229M	1/16kHz	×	84.6	2.56	0.23	1.23
SpecMaskFoley (Zhong et al., 2025)	300M	1/22.05kHz	$\checkmark$	109	1.76	0.26	0.65
Seeing & Hearing (Xing et al., 2024)	415M	1/16kHz	$\checkmark$	219	2.30	0.34	1.20
ReWaS (Jeong et al., 2024)	620M	1/16kHz	$\checkmark$	141	2.82	0.15	1.06
MMAudio-L (Cheng et al., 2025)	1.03B	1/44.1kHz	$\checkmark$	60.6	1.40	0.33	0.44
FoleyCrafter (Zhang et al., 2024)	1.22B	1/16kHz	✓	140	2.23	0.26	1.23
Frame-level online models (Ours)							_
SoundReactor-Diffusion	336M	2/48kHz	×	175	2.37	0.21	1.04
SoundReactor-ECT (NFE=1)	336M	2/48kHz	×	194	2.37	0.21	1.03
SoundReactor-ECT (NFE=2)	336M	2/48kHz	×	130	2.32	0.24	1.02
SoundReactor-ECT (NFE=4)	336M	2/48kHz	×	113	2.37	0.24	1.03

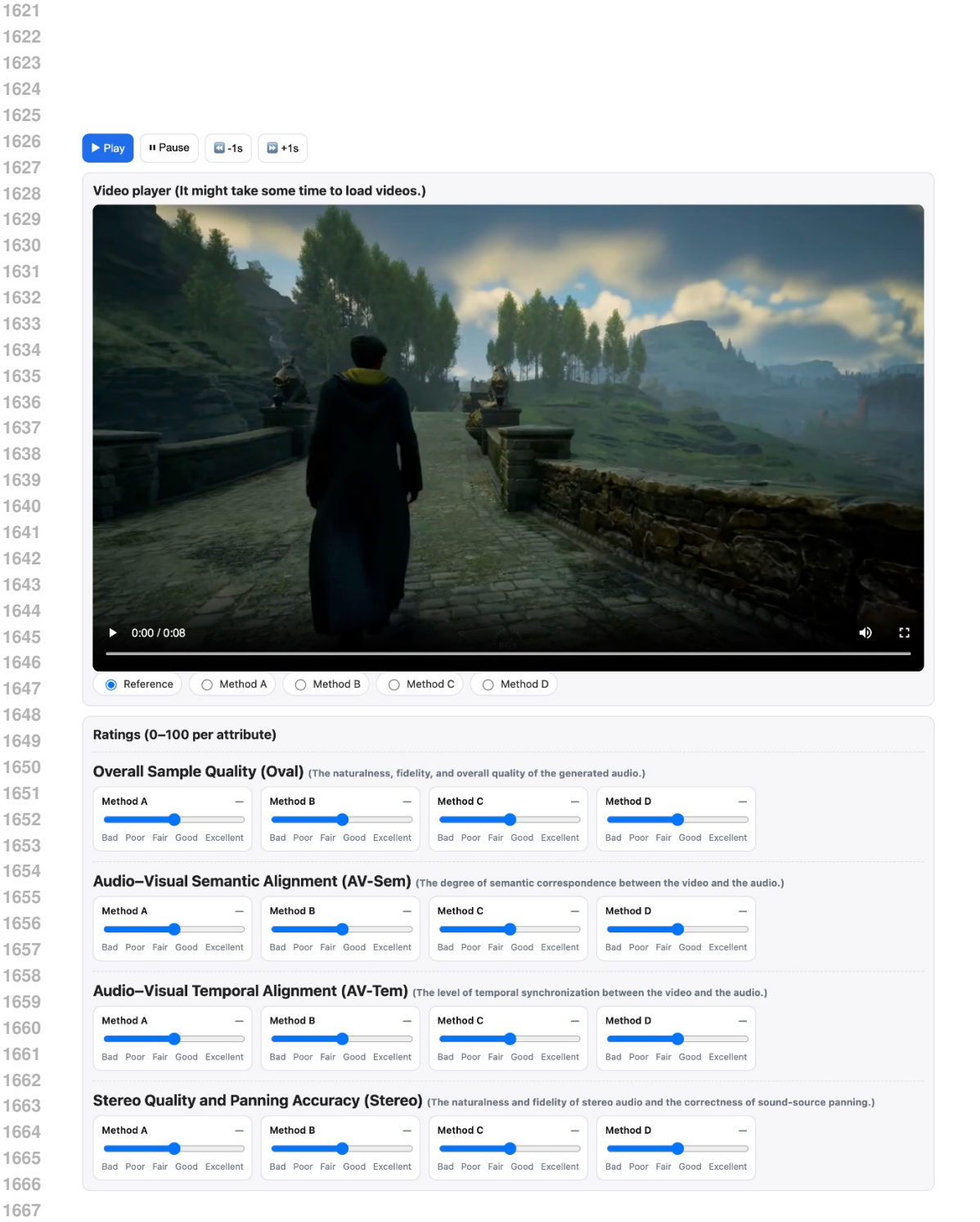


Figure 9: Screenshot of human evaluation